

University of Windsor

## Scholarship at UWindor

---

Electronic Theses and Dissertations

Theses, Dissertations, and Major Papers

---

10-30-2020

# Adaptive Indoor Pedestrian Tracking Using Foot-Mounted Miniature Inertial Sensor

Ravindra Kumar Dhanapal  
*University of Windsor*

Follow this and additional works at: <https://scholar.uwindsor.ca/etd>

---

### Recommended Citation

Dhanapal, Ravindra Kumar, "Adaptive Indoor Pedestrian Tracking Using Foot-Mounted Miniature Inertial Sensor" (2020). *Electronic Theses and Dissertations*. 8445.  
<https://scholar.uwindsor.ca/etd/8445>

This online database contains the full-text of PhD dissertations and Masters' theses of University of Windsor students from 1954 forward. These documents are made available for personal study and research purposes only, in accordance with the Canadian Copyright Act and the Creative Commons license—CC BY-NC-ND (Attribution, Non-Commercial, No Derivative Works). Under this license, works must always be attributed to the copyright holder (original author), cannot be used for any commercial purposes, and may not be altered. Any other use would require the permission of the copyright holder. Students may inquire about withdrawing their dissertation and/or thesis from this database. For additional inquiries, please contact the repository administrator via email ([scholarship@uwindsor.ca](mailto:scholarship@uwindsor.ca)) or by telephone at 519-253-3000ext. 3208.

**ADAPTIVE INDOOR PEDESTRIAN TRACKING USING  
FOOT-MOUNTED MINIATURE INERTIAL SENSOR**

by

Ravindra Kumar Dhanapal

A Thesis

Submitted to the Faculty of Graduate Studies  
through the Department of Electrical and Computer Engineering  
in Partial Fulfilment of the Requirements for  
the Degree of Master of Applied Science at the  
University of Windsor

Windsor, Ontario, Canada

© 2020 Ravindra Kumar Dhanapal

ADAPTIVE INDOOR PEDESTRIAN TRACKING USING FOOT-MOUNTED  
MINIATURE INERTIAL SENSOR

by  
Ravindra Kumar Dhanapal

APPROVED BY:

---

Y.H.Kim  
Department of Civil and Environmental Engineering

---

A.Emadi  
Department of Electrical and Computer Engineering

---

B.Balasingam, Advisor  
Department of Electrical and Computer Engineering

September 08, 2020

# Declaration of Co-Authorship / Previous Publication

## I. Co-Authorship

I hereby declare that this dissertation incorporates material that is result of joint research, as follows: This dissertation incorporates a joint research undertaken with J.Wang, P.Ramakrishnan and professor B.Balasingam from University of Windsor along with T.Souza and R.Maev from Institute for Diagnostic Imaging Research in Chapter 1. Chapters 2, 3, 4 and 5 of this thesis were co-authored with professor B.Balasingam who provided supervision and guidance during the research and writing process. In all chapters, the key ideas, primary contributions, data analysis, interpretation, and writing were performed by the author.

I am aware of the University of Windsor Senate Policy on Authorship and I certify that I have properly acknowledged the contribution of other researchers to my dissertation, and have obtained written permission from each of the co-author(s) to include the above material(s) in my dissertation.

I certify that, with the above qualification, this dissertation, and the research to which it refers, is the product of my own work.

## II. Previous Publication

This thesis includes 2 original papers that have been previously published/submitted for publication in peer reviewed journals, as follows:

Thesis chapter	Publication title/full citation	Publication status
1	Wang, Jingyu & <b>Dhanapal, Ravindra Kumar</b> & Ramakrishnan, Priyadharshini & Balasingam, Balakumar & Souza, Thiago & Maev, Roman. “Active RFID Based Indoor Localization”, 22 <sup>nd</sup> International Conference on Information Fusion, July 2019	Published
1	Wang, Jingyu & <b>Dhanapal, Ravindra Kumar</b> & Ramakrishnan, Priyadharshini & Balasingam, Balakumar. “Quickest Detection of Abnormal Vehicle Movements on Highways”, 22 <sup>nd</sup> International Conference on Information Fusion, July 2019.	Published
2, 3, 4, 5	<b>Dhanapal, Ravindra Kumar</b> & Balasingam, Balakumar. “Adaptive Indoor Pedestrian Tracking Using Foot-Mounted Miniature Inertial Sensor”.	To be submitted

I certify that I have obtained a written permission from the copyright owner(s) to include the above published material(s) in my thesis. I certify that the above material describes work completed during my registration as a graduate student at the University of Windsor.

### III. General

I declare that, to the best of my knowledge, my thesis does not infringe upon anyone's copyright nor violate any proprietary rights and that any ideas, techniques, quotations, or any other material from the work of other people included in my thesis, published or otherwise, are fully acknowledged in accordance with the standard referencing practices. Furthermore, to the extent that I have included copyrighted material that surpasses the bounds of fair dealing within the meaning of the Canada Copyright Act, I certify that I have obtained a written permission from the copyright owner(s) to include such material(s) in my thesis.

I declare that this is a true copy of my thesis, including any final revisions, as approved by my thesis committee and the Graduate Studies office, and that this thesis has not been submitted for a higher degree to any other University or Institution.

# Abstract

This dissertation introduces a positioning system for measuring and tracking the momentary location of a pedestrian, regardless of the environmental variations. This report proposed a 6-DOF (degrees of freedom) foot-mounted miniature inertial sensor for indoor localization which has been tested with simulated and real-world data. To estimate the orientation, velocity and position of a pedestrian we describe and implement a Kalman filter (KF) based framework, a zero-velocity updates (ZUPTs) methodology, as well as, a zero-velocity (ZV) detection algorithm. The novel approach presented in this dissertation uses the interactive multiple model (IMM) filter in order to determine the exact state of pedestrian with changing dynamics.

This work evaluates the performance of the proposed method in two different ways: At first a vehicle traveling in a straight line is simulated using commonly used kinematic motion models in the area of tracking (constant velocity (CV), constant acceleration (CA) and coordinated turn (CT) models) which demonstrates accurate state estimation of targets with changing dynamics is achieved through the use of multiple model filter models. We conclude by proposing an interactive multiple model estimator based adaptive indoor pedestrian tracking system for handling dynamic motion which can incorporate different motion types (walking, running, sprinting and ladder climbing) whose threshold is determined individually and IMM adjusts itself adaptively to correct the change in motion models. Results indicate that the overall IMM performance will at all times be similar to the best individual filter model within the IMM.

# Contents

<b>Declaration of Co-Authorship / Previous Publication</b>	<b>iii</b>
<b>Abstract</b>	<b>vi</b>
<b>List of Tables</b>	<b>x</b>
<b>List of Figures</b>	<b>xi</b>
<b>1 INTRODUCTION</b>	<b>1</b>
1.1 Pedestrian Navigation: General Overview . . . . .	1
1.2 Sensors Used for Autonomous Detection and Tracking . . . . .	3
1.2.1 RADAR: <b>R</b> Adio <b>D</b> etection <b>A</b> nd <b>R</b> anging . . . . .	3
1.2.2 LiDAR: <b>L</b> ight <b>D</b> etection <b>A</b> nd <b>R</b> anging . . . . .	4
1.2.3 SONAR: <b>S</b> Ound <b>N</b> avigation <b>A</b> nd <b>R</b> anging . . . . .	4
1.2.4 IR: <b>I</b> nfrared <b>R</b> adiation . . . . .	4
1.2.5 RFID: <b>R</b> adio <b>F</b> requency <b>I</b> Dentification . . . . .	5
1.2.6 Ultrasonic . . . . .	5
1.2.7 Video Camera . . . . .	6
1.2.8 IMU: <b>I</b> nertial <b>M</b> easurement <b>U</b> nit . . . . .	6
1.3 Motivation for Tracking Using Inertial Sensors . . . . .	6
1.4 Background . . . . .	7
1.5 Methodology . . . . .	9
1.6 Dissertation Outline . . . . .	9

1.7	System Overview . . . . .	10
1.8	Bibliography . . . . .	13
<b>2</b>	<b>INERTIAL NAVIGATION SYSTEM</b>	<b>15</b>
2.1	Human gait Cycle . . . . .	15
2.2	Inertial Sensors Used for Detecting Human gait . . . . .	17
2.2.1	Accelerometer . . . . .	17
2.2.2	Gyroscope . . . . .	17
2.2.3	Magnetometer . . . . .	18
2.3	MEMS Technology . . . . .	18
2.4	The Mathematics Of Inertial Navigation . . . . .	19
2.4.1	Accelerometer Model . . . . .	19
2.4.2	Gyroscope Model . . . . .	20
2.5	Attitude Representation . . . . .	21
2.5.1	Euler Angles . . . . .	21
2.5.2	Quaternions . . . . .	25
2.6	Coordinate Systems and Transformations . . . . .	25
2.6.1	Sensor Frame (s-frame) . . . . .	26
2.6.2	Global Frame (g-frame) . . . . .	27
2.6.3	Coordinate Frame Transformation . . . . .	28
2.7	Correcting Inertial Navigation . . . . .	30
2.7.1	Error Types: MEMS Accelerometers and Gyroscopes Sources of Error . . . . .	30
2.7.2	Environmental Influences on Quality of Data Collected . . . . .	31
2.8	Bibliography . . . . .	33
<b>3</b>	<b>THEORY OF ADAPTIVE ESTIMATION</b>	<b>34</b>
3.1	Calibration . . . . .	34
3.2	The Kalman Filter (KF) . . . . .	35

3.2.1	The Standard Kalman Filtering Algorithm . . . . .	35
3.2.2	Implementing Kalman Filter . . . . .	37
3.2.3	Performance Analysis . . . . .	38
3.2.4	Conclusion . . . . .	39
3.3	Interactive Multiple Model (IMM) . . . . .	41
3.3.1	The Standard Interactive Multiple Model (IMM) Algorithm . . . . .	42
3.3.2	Implementing Interactive Multiple Model (IMM) . . . . .	47
3.3.3	Performance Comparison . . . . .	52
3.3.4	Conclusions . . . . .	54
3.4	Bibliography . . . . .	56
<b>4</b>	<b>EXPERIMENTAL RESULTS AND DISCUSSION</b>	<b>57</b>
4.1	Zero Velocity Detection . . . . .	57
4.2	Zero Velocity Updates (ZUPTS) . . . . .	58
4.3	Description of the Data . . . . .	60
4.4	Demonstration of Pedestrian Tracking Using KF While Walking . . . . .	61
4.5	Demonstration of Pedestrian Tracking Using KF While Running . . . . .	63
4.6	Adaptive Tracking Using IMM Estimator . . . . .	65
4.7	Bibliography . . . . .	67
<b>5</b>	<b>SUMMARY AND FUTURE WORK</b>	<b>68</b>
5.1	Summary . . . . .	68
5.2	Future Work . . . . .	70
5.3	Bibliography . . . . .	72
	<b>Appendices</b>	<b>74</b>
	<b>Vita Auctoris</b>	<b>78</b>

# List of Tables

2.1	Accelerometer Error Sources . . . . .	31
2.2	Gyroscope Error Sources . . . . .	32

# List of Figures

1.1	<b>Structure of thesis</b> Logical interconnections among chapters. . . .	11
1.2	<b>Closed loop implementation of ZUPT aided inertial navigation system.</b> A schematic description of the proposed system with its input and output signals. . . . .	12
2.3	<b>Human gait cycle divided into two phases: stance and stride.</b> Inertial sensor mounted on foot for gait cycle extraction. . . . .	16
2.4	<b>Rotating a vector, (A).</b> Polar and cartesian coordinates systems.	22
2.5	<b>Three-dimensional coordinate frame.</b> Standard x-y-z coordinate frame. . . . .	24
2.6	<b>Global frame reference coordinate system.</b> g-frame. . . . .	27
3.7	<b>Kalman filter Algorithm</b> A block diagram of the KF algorithm. . .	36
3.8	<b>Recursively estimating the state of vehicle B with respect to vehicle A.</b> Using Kalman filtering Algorithm. . . . .	38
3.9	<b>States of vehicle B are plotted.</b> (a) True position, measured position and estimated position (KF) (b) True velocity, estimated velocity (KF) and (c) True acceleration, estimated acceleration (KF). . . . .	39
3.10	<b>Estimating the error covariance of vehicle B.</b> (a) Position error covariance (b) Velocity error covariance and (c) Acceleration error covariance. . . . .	40

3.11	<b>Normalised Innovations Squared (NIS)</b> Used to check the consistency of Kalman filter. . . . .	41
3.12	<b>Interactive Multiple Model Algorithm.</b> A block diagram of the IMM algorithm with two filter models. . . . .	45
3.13	<b>Data is simulated using constant velocity model for a vehicle moving in straight line.</b> Model probability of two interactive multiple model filters are compared i.e. constant velocity and constant acceleration. . . . .	49
3.14	<b>Data is simulated using constant velocity model for a vehicle moving in straight line.</b> RMS rate error of constant velocity and constant acceleration are compared to number of samples (N=500). . . . .	50
3.15	<b>Data is simulated using coordinated turn model for a vehicle moving in straight line.</b> Model probability of two interactive multiple model filters are compared i.e. coordinated turn and constant acceleration. . . . .	52
3.16	<b>Data is simulated using coordinated turn model for a vehicle moving in straight line.</b> RMS rate error of coordinated turn and constant acceleration are compared to number of samples (N=500). . . . .	53
4.17	<b>Block diagram for swing and stance phase detection.</b> Angular velocity is examined for zero velocity detection. . . . .	58
4.18	<b>Zero velocity update block diagram.</b> The block diagram illustrates the components and their relations of a ZUPT-aided INS system. . . . .	59
4.19	<b>Hallway Test Course.</b> Ground truth obtained using Leica M500 Multistation along with the marker [2]. . . . .	60
4.20	<b>Demonstration of Pedestrian Tracking Using KF While Walking.</b> Estimated two dimensional path tracked using ZUPT. . . . .	62
4.21	<b>Estimated Distance Travelled.</b> This graph represents total time taken v/s Total distance travelled for a walking framework. . . . .	63

4.22	<b>Demonstration of Pedestrian Tracking Using KF While Running.</b> Estimated 2D path tracked using ZUPT. . . . .	64
4.23	<b>Estimated Distance Travelled.</b> This graph represents total time taken v/s Total distance travelled for a running framework. . . . .	65
24	<b>Accelerometer data passed through low pass filter.</b> Accelerometer measurements when passed through low pass filter helps in improving jitter correction. . . . .	76
25	<b>Gyroscope data passed through high pass filter.</b> Gyroscope measurements when passed through high pass filter helps in correcting the drift. . . . .	77
26	<b>Gesture Reconstruction.</b> Experimental results of our proposed method for handwritten number reconstruction. . . . .	77

# Chapter 1

## INTRODUCTION

### 1.1 Pedestrian Navigation: General Overview

The problem of geolocation in an open environment is relatively simple using global positioning system (GPS), which has been developed for outdoor application to determine the ground position of an object. Most of the location-based service such as air traffic control, vehicle navigation system, and pedestrian navigation are based on the use of GPS receptors. GPS signals are not always available because they can be blocked by high raised buildings, canyons or forests among others. This thesis introduces a navigation system for tracking location and trajectory of a pedestrian even if GPS, beacons and landmarks are not available. Such a system is useful in GPS-denied environments such as, indoor navigation, emergency response, and military applications.

This work extends prior work done on indoor pedestrian navigation using inertial sensors in order to overcome problems of limited range, portability and line-of-sight restrictions. The inertial navigation system (INS) gives a solution for pedestrian navigation by using inertial measurement unit (IMU) which provide acceleration and

angular velocity measurements that are used to estimate the location of the pedestrian relative to a known starting point. IMU normally contains several accelerometers, gyroscope, magnetometers and even pressure sensors. The IMU sensors used in aerospace applications are bulky, but they provide very accurate measurements with a low drift. The size and performance of an inertial sensor are linearly dependent parameter, i.e., the smaller the sensor the lower the measurement accuracy. Smaller IMU units such as those based on micro-electro-mechanical system (MEMS) sensors are becoming very popular, but they have significant noise and bias and therefore suffer large errors in navigation [1].

Recent advancement in MEMS technology have brought about the development of inertial sensors with dimensions in several hundred-micron range, modest performance and with very low cost. The main advantage of inertial sensor-based system is that they are environment-independent compared to other pedestrian navigation systems which uses vision or wireless communication that may require landmark or wireless nodes to be installed in the environment well in advance [2]. The development of a low-cost miniature MEMS-based inertial navigation, augmented with GPS, provides sufficient accuracy to determine the location of pedestrian, whether obscured in the open or in a large building complex.

In addition to IMU and GPS, several other sensors are useful in autonomous navigation of vehicles, robots and humans. Some of them are briefly introduced in the next few subsections. The challenges faced by all of them are similar! how to improve their localization and tracking performance given the measurement noise, bias, and blackouts?

## 1.2 Sensors Used for Autonomous Detection and Tracking

A device that detects the changes in electrical, physical or other quantities and thereby produces an output as an acknowledgement of change in the quantity is called as a sensor. The most frequently used types of sensors to detect the presence of an object are RADAR, LiDAR, SONAR, IR, RFID, Ultrasonic and Video Camera. Brief description about these sensors along with their applications are as discussed.

### 1.2.1 RADAR: RAdio Detection And Ranging

Radar is an electromagnetic system used for detection and location of objects. It operates by radiating energy into space and monitoring the echo or reflected signals from the objects.

The radar system generally consists of a transmitter which produces an electromagnetic signal that is radiated into space by an antenna. When this signal strikes any object, it gets reflected or reradiated in many directions. This reflected or echo signal is received by the radar antenna which delivers it to the receiver, where it is processed to determine the geographical position statistics of the object. The range to the object is determined by measuring the time taken for the radar signal to travel to the object and back. The direction, or angular position, of the object may be determined from the direction of arrival of the reflected wavefront.

One of our paper published at international conference on information fusion 2019, is about the use of radars for autonomous vehicle navigation. In this paper, we present an approach to quickly detect lane-changing maneuvers of a nearby vehicle using simulated radar measurement [3].

### **1.2.2 LiDAR: Light Detection And Ranging**

LiDAR is a remote detection and ranging method that works much like radar, emitting infrared light pulses instead of radio waves and measuring how long they take to come back after hitting nearby objects. The time between the output laser pulse and the reflected pulse allows the LiDAR sensor to calculate the distance to each object precisely, based on the speed of light.

LiDAR captures millions of such precise distance measurement points each second, from which a three-dimensional representation of its environment can be produced. Information on object's position, shape, and behavior can be obtained from this comprehensive mapping of the environment.

### **1.2.3 SONAR: SOund Navigation And Ranging**

Sonar is a technique for detecting and determining the distance and direction of objects by acoustic means. Sound waves emitted by or reflected from the object are detected by sonar apparatus and analyzed for the information they contain.

An ultrasonic pulse wave is transmitted by the transducer, which immediately switches into a receiving mode. After receiving the returned echo, the transducer turns to the left or right and transmits a new burst of ultrasonic waves in a cyclic operation. Anything that gets hit by these ultrasonic waves will give a returning echo that shows up on the sonar display.

### **1.2.4 IR: Infrared Radiation**

Infrared is electromagnetic radiation with wavelengths longer than those of a visible light. Although infrared radiation is not visible, it can be measured as heat.

An infrared sensor is an electronic instrument that is used to sense certain characteristics of its surroundings. Infrared sensors are capable of measuring the heat being emitted by an object which is used for night vision and navigation.

### **1.2.5 RFID: Radio Frequency IDentification**

RFID methods utilize radio waves to automatically identify objects, collect data about them, and enter those data directly into computer systems with little or no human intervention. At a simple level, RFID systems consist of three components: an RFID tag or smart label, an RFID reader, and an antenna. RFID tags contain an integrated circuit and an antenna, which are used to transmit data to the RFID reader. In a typical operation, RFID antenna sends a signal and listens the reflections from RFID tags based on the strength of the received signal, the location of the tag can be computed this is known as passive RFID system. In active RFID system, the tags are equipped power supplies and can improve the detection range.

One of our paper published at international conference on information fusion 2019, illustrates the use of an active RFID for indoor localization [4]. The performance of real-time RFID based localization system is implemented by using an extended Kalman filter (EKF).

### **1.2.6 Ultrasonic**

An ultrasonic sensor is an electronic device that measures the distance of a target object by emitting ultrasonic sound waves and converts the reflected sound into an electrical signal. Ultrasonic sensors have two main components: the transmitter (which emits the sound using piezoelectric crystals) and the receiver (which encounters the reflected sound from the target).

In order to calculate the distance between the sensor and the object, the sensor measures the time it takes between the emission of the sound by the transmitter to its contact with the receiver. Ultrasonic sensors are used primarily as proximity sensors. They can be found in automobile self-parking technology or anti-collision safety systems [5], and robotic obstacle detection systems [6]. They are also used as level sensors to detect, monitor, and regulate liquid levels in closed containers. Most

notably, ultrasonic technology has enabled the medical industry to produce images of internal organs, identify tumors, and ensure the health of babies in the womb.

### **1.2.7 Video Camera**

Video tracking is the process of locating a moving object (or multiple objects) over time using a camera. It has a variety of uses, some of which are: human-computer interaction, security and surveillance, video communication, augmented reality, traffic control, medical imaging and video editing. Video tracking can be a time-consuming process due to the amount of data that is contained in video. With the use of computer vision, video tracking has the potential to emulate human vision in a vast array of practical applications. Further, video-based sensors also have applications in monitoring and tracking aerospace and astronomic objects.

### **1.2.8 IMU: Inertial Measurement Unit**

An inertial measurement unit works by detecting linear acceleration using one or more accelerometers and rotational rate using one or more gyroscopes. Some also include a magnetometer which is commonly used as a heading reference. Typical configurations contain one accelerometer, gyroscope and magnetometer per axis for each of the three principal axes: pitch, roll and yaw. The focus of this thesis about IMU based navigation - more details will follow in the subsequent chapters.

## **1.3 Motivation for Tracking Using Inertial Sensors**

Indoor-pedestrian navigation system that tracks the location of a pedestrian with a foot-mounted IMU has several applications, such as, finding and rescuing firefighter's or emergency first responders, location-aware computing, pedestrian navigation assistance, mobile 3D audio, and mixed or augmented reality applications. One of the

main obstacles to the real-world deployment of location sensitive wearable computing, including mixed reality, is that current position tracking technologies require an instrumented, marked, or pre-mapped environment. Installing markers or instrumentation in advance is impractical for many mobile applications, and there is an intense search for a tracking method that will work reliably without preparation in any indoor or outdoor setting [7].

Additional applications of inertial sensors include using a yaw rate sensor for skid control in anti-lock braking applications for automobiles, adding a lateral accelerometer to the gyroscope provides the capability to conduct real time suspension control improving better handling, stability, and ride optimization [2].

## 1.4 Background

Reliable localization has been the center for pedestrian navigation systems. Pedestrian dead-reckoning (PDR) using foot mounted IMUs is the basis for many indoor localization techniques, including map matching, various types of simultaneous localization and mapping (SLAM), and integration with GPS. Pedestrian navigation systems has been implemented with numerous types of sensors and algorithm, the focus of these system is to compute accurate position information of a person indoors or outdoors for example if the application permits the installation of fiducials ahead of time then the use of computer vision for position estimation is justified where images are compared and matched against a pre-compiled database this approach requires very large database but the results obtained are satisfying [9]. Simultaneous Location and Mapping (SLAM) systems which do not require a pre-compiled database can be used for indoor tracking, but the poor visibility and unfavourable lighting conditions can result in completely false position estimation [10]. Use of ultrasonic sensors attached to the user's boots are also studied and found that sensor requires a direct line of sight between boots, which may be a problem on rough terrain [11]. In order

to overcome problems of limited range, portability, line of sight restrictions, and self-contained source less tracking system the use of inertial sensors was preferred over the other forms of indoor tracking. The earlier versions of system used an impractically larger IMU. The advancement of MEMS inertial sensor has drastically improved the ability of inertial sensor to shrink to extreme small size. The advancement of low-cost miniature inertial sensors has opened a reliable use for indoor pedestrian navigation systems constructed around foot-mounted inertial sensors.

We propose a system to track position based on inertial sensors. The wireless inertial sensor is small enough to easily be placed on the boot and consume sufficiently low power to run on a small battery. When a person walks, their feet alternates between a stationary stance phase and a moving stride phase, our approach detects the stationary stance phase and applies zero-velocity updates as pseudo-measurements into Kalman filter. This allows the KF to correct the velocity error after each stride. Over time the estimate become less accurate, because they rely on previous estimates, which are imperfect due to errors in speed and heading measurements. In other words, small error in heading and speed accumulate to form an increasingly large error in the position estimate [12].

It is very common to use external sensors such as radio frequency sensors, optical trackers, and pressure sensors for calculating the period when a single foot is carrying the full weight of the body [13]. The sensors, either an accelerometer or a gyroscope or both, are used to detect a static period of gait i.e., magnitude, moving average, variance, and RMS values of an accelerometer are adopted to detect the stand-still stage of pedestrian also gyroscope output is used to calculate its magnitude, RMS and moving average most of the mentioned methods are based on thresholding to determine desired event some approaches use machine learning techniques such as LSTM, SVM, k-NN [14–16]. To create a more robust zero velocity detector that works across a range of motion types we propose an IMM filter that estimates changing dynamics through the use of multiple filter models as it provides a structure to efficiently

manage individual filter parameters.

## 1.5 Methodology

Over past few years, there has been a consistent effort to make indoor navigation more efficient. This thesis designs, develops and assesses a more accurate algorithm to estimate the position of a pedestrian over a dynamic motion using accelerometers and gyroscopes.

First, the position, velocity and orientation are recursively estimated by fusing acceleration and angular velocity measurements from inertial sensor furthermore Euler angle (pitch, roll and yaw) are used to describe the orientation of the sensor with respect to a fixed coordinate system. Second, we used gyroscope zero velocity thresholding along with ZUPTs to precisely detect the stand still phase in a human gait. Finally, in the end we use adaptive estimation theory i.e. IMM algorithm along with Kalman filtering to get a better state estimate of targets with changing dynamics.

The Novelty of the proposed algorithm is the use of multiple model filter models that can maintain high accuracy and robustness on motion trajectory under various dynamic activity, such as walking, jogging, running, crawling. This algorithm has been experimentally verified for real-world measurements. Thus, this method gives an accurate state estimation of the pedestrian in an indoor environment.

## 1.6 Dissertation Outline

The structure of this dissertation is divided into five chapters.

- Chapter one provides a general overview on pedestrian tracking along with different types of sensors used for detection and tracking objects autonomously, this is then followed by thesis objective, background and the outline of the dissertation.

- Chapter two presents the introduction to human gait analysis, MEMS technology and the mathematics of inertial navigation where in the attitude representation, coordinate systems and transformation are studied. In the very end of this chapter we go through different errors types which might frequently occur in IMU along with the environment influences on the quality of data collected.
- Chapter three reviews the basic principle of adaptive estimation theory starting with the Kalman filters and then followed by IMM, both Kalman filter and IMM are implemented and a comprehensive performance analysis is discussed. The performance of the IMM is tested using different models this includes constant velocity (CV), constant acceleration (CA) and coordinated turn (CT) motion models.
- Chapter four presents zero velocity detection and ZUPT along with the results using IMM algorithm. Results from real world data are presented and discussed.
- Chapter five summarize the contributions of the thesis, and lists the possible directions of future research.

Logical interconnections among chapters are illustrate in figure 1.1.

## 1.7 System Overview

This dissertation proposes a method for indoor navigation which has been tested with real world data. When a person walks, their feet alternates between stationary stance phase and moving stride phase. Our algorithm applies gyroscope thresholding to detects the stationary stance phases of a gait cycle and the ZUPT is implemented as closed-loop system, where the zero velocity updates are used as pseudo velocity observation for a Kalman filter that estimates the errors in the navigation system. Introduces ZUPTs as measurement into the Kalman filter instead of simply resetting the velocity to zero in the inertial integrator achieves important benefits like the ZUPT

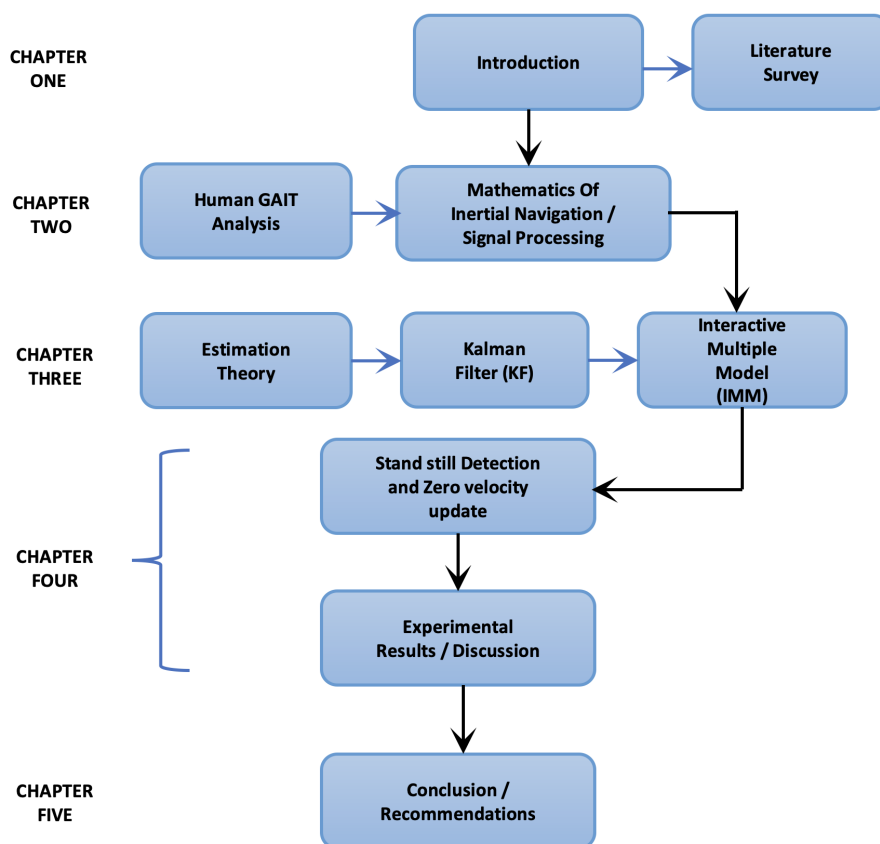


Figure 1.1: **Structure of thesis** Logical interconnections among chapters.

lets the Kalman filer retroactively correct most of the position drift that occurs during the moving stride phase.

Figure 4.18, depicts closed loop implementation of ZUPT aided inertial navigation system. Detailed implementation of a zero-velocity aided inertial navigation system can be found in the upcoming chapters.

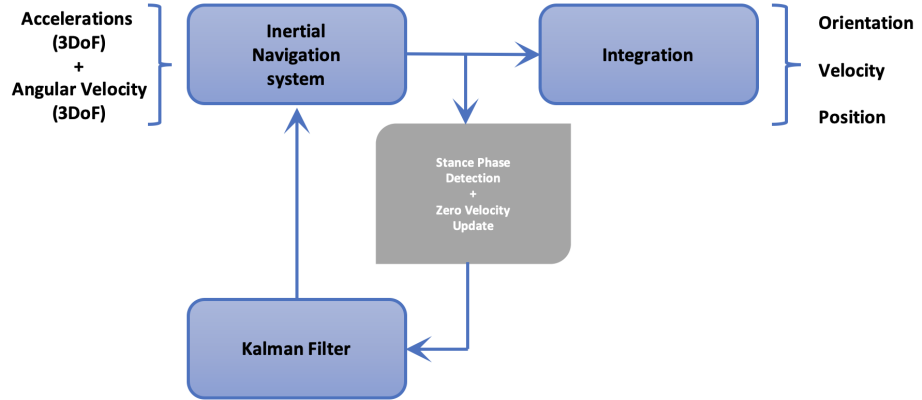


Figure 1.2: **Closed loop implementation of ZUPT aided inertial navigation system.** A schematic description of the proposed system with its input and output signals.

## 1.8 Bibliography

- [1] A. R. Jiménez, F. Seco, J. C. Prieto, and J. Guevara, “Indoor pedestrian navigation using an ins/ekf framework for yaw drift reduction and a foot-mounted imu,” in *2010 7th Workshop on Positioning, Navigation and Communication*, 2010. pages 2, 59, 70
- [2] A. Kourepenis, J. Borenstein, J. Connelly, R. Elliott, P. Ward, and M. Weinberg, “Performance of mems inertial sensors,” in *IEEE 1998 Position Location and Navigation Symposium (Cat. No. 98CH36153)*, 1996. pages 2, 7
- [3] J. Wang, R. K. Dhanapal, P. Ramakrishnan, and B. Balasingam, “Quickest detection of abnormal vehicle movements on highways,” in *2019 22th International Conference on Information Fusion (FUSION)*, 2019. pages 3
- [4] J. Wang, R. K. Dhanapal, P. Ramakrishnan, B. Balasingam, T. Souza, and R. Maev, “Active rfid based indoor localization,” in *2019 22th International Conference on Information Fusion (FUSION)*, 2019. pages 5
- [5] A. L. Favors, “Anti-collision sensor,” 1990. US Patent 4,928,101. pages 5
- [6] S. Shoval and J. Borenstein, “Using coded signals to benefit from ultrasonic sensor crosstalk in mobile robot obstacle avoidance,” in *Proceedings 2001 ICRA. IEEE International Conference on Robotics and year=2001*. pages 5
- [7] E. Foxlin, “Pedestrian tracking with shoe-mounted inertial sensors,” *IEEE Computer graphics and applications*, 2005. pages 7
- [8] Y. Bar-Shalom, X. R. Li, and T. Kirubarajan, *Estimation with applications to tracking and navigation: theory algorithms and software*. 2004. pages 42
- [9] Y. Watanabe, T. Hatanaka, T. Komuro, and M. Ishikawa, “Human gait estimation using a wearable camera,” in *2011 IEEE Workshop on Applications of Computer Vision (WACV)*, 2011. pages 7

- [10] M. Angermann and P. Robertson, “Footslam: Pedestrian simultaneous localization and mapping without exteroceptive sensors—hitchhiking on human perception and cognition,” *Proceedings of the IEEE*, 2012. pages 7
- [11] J. Saarinen, J. Suomela, S. Heikkila, M. Elomaa, and A. Halme, “Personal navigation system,” in *2004 IEEE/RSJ International Conference on Intelligent Robots and Systems (IROS)(IEEE Cat. No. 04CH37566)*, 2004. pages 7
- [12] C. Fischer, P. T. Sukumar, and M. Hazas, “Tutorial: Implementing a pedestrian tracker using inertial sensors,” *IEEE pervasive computing*, 2012. pages 8
- [13] C. Zhou, J. Downey, J. Choi, D. Stancil, J. Paramesh, and T. Mukherjee, “A shoe-embedded rf sensor for motion detection,” *IEEE Microwave and wireless components letters*, 2011. pages 8
- [14] I. Skog, P. Handel, J.-O. Nilsson, and J. Rantakokko, “Zero-velocity detection—an algorithm evaluation,” *IEEE transactions on biomedical engineering*, 2010. pages 8, 61, 70
- [15] S. Y. Park, H. Ju, and C. G. Park, “Stance phase detection of multiple actions for military drill using foot-mounted imu,” *sensors*, 2016. pages 8, 70
- [16] B. Wagstaff and J. Kelly, “Lstm-based zero-velocity detection for robust inertial navigation,” in *2018 International Conference on Indoor Positioning and Indoor Navigation (IPIN)*, 2018. pages xii, 8, 60, 70

# Chapter 2

## INERTIAL NAVIGATION SYSTEM

### 2.1 Human gait Cycle

For humans, walking is the most basic method of movement and gait is a person's pattern of walking. A method to detect stance and stride gait phases using single IMU attached to the foot is proposed. Normal forward walking consists of two phases: stance and stride.

- Stance phase occupies 60 % of the gait cycle, during which one leg bears most or all of the body weight.
- Stride phase occupies only 40 % of it gait cycle, during which the foot is not touching the walking surface and the body weight is borne by the other leg and foot.
- In a complete two-step cycle both feet are in contact with the floor at the same time for about 25 per cent of the time. This part of the cycle is called the double-support phase [1].

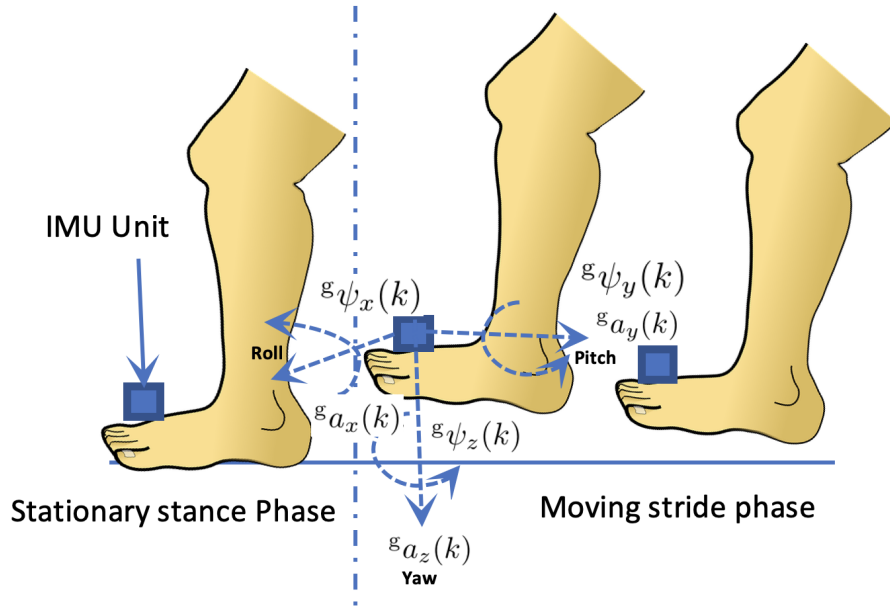


Figure 2.3: **Human gait cycle divided into two phases: stance and stride.** Inertial sensor mounted on foot for gait cycle extraction.

Human gait depends on a complex interplay of major parts of the nervous, musculoskeletal and cardiorespiratory systems [1].

- The individual gait pattern is influenced by age, personality, mood and socio-cultural factors.
- The preferred walking speed in older adults is a sensitive marker of general health and survival.
- Safe walking requires intact cognition and executive control.
- Gait disorders lead to a loss of personal freedom, falls and injuries and result in a marked reduction in the quality of life.

The overall conceptual diagram to detect stance phase of multi-action is shown in figure 2.3. However, the current gait phase analysis is done based on visual inspection or visual odometry. Therefore, there is a need for autonomous gait phase detection.

In this thesis, the technique for finding the time when foot is in contact with ground is studied in detail i.e., gait phase detection is essential to examine the zero-velocity detection of pedestrian.

## **2.2 Inertial Sensors Used for Detecting Human gait**

Gait phase detection is essential to examine the gait cycle of a pedestrian. The importance of gait phase identification is that it is one of the methods used to evaluate and diagnose indoor localization. The Inertial sensors are strapped to foot using Velcro straps. The sensors, either an accelerometer or a gyroscope or both are used to detect a stance phase of gait. An IMU is a specific type of sensor that measures angular rate, force and sometimes magnetic field. IMUs are composed of a 3-axis accelerometer and a 3-axis gyroscope, which would be considered a 6-axis IMU. Different types of motion sensors used in IMU will be discussed as follows.

### **2.2.1 Accelerometer**

The most commonly used type of motion sensor is the accelerometer. It measures acceleration (rate of change of velocity) across all the x, y and z axis. An accelerometer can also be used to measure gravity as a downward force. Integrating acceleration once reveals an estimate for velocity and integrating again gives an estimate for position.

### **2.2.2 Gyroscope**

While accelerometers can measure linear acceleration, they can't measure twisting or rotational movement. Gyroscopes, however, measure angular velocity about three axes: pitch (x-axis), roll (y-axis) and yaw (z-axis). Gyroscope measurements are integrated to determine an object's orientation within three-dimensional space.

### 2.2.3 Magnetometer

A magnetometer measures magnetic field. It can detect fluctuations in Earth's magnetic field, by measuring magnetic flux density at the sensor's point in space. Through those fluctuations, it finds the vector towards Earth's magnetic North. This can be fused in conjunction with accelerometer and gyroscope data to determine absolute heading.

IMUs are used to measure acceleration, angular velocity and magnetic fields and when combined with sensor fusion techniques, they can be used to determine and track the exact position, velocity, and acceleration of the object on the surface of earth.

## 2.3 MEMS Technology

Micro-Electro-Mechanical Systems (MEMS) is a technology that in its most general form can be defined as miniaturized mechanical and electro-mechanical elements (i.e., devices and structures) that are made using the techniques of microfabrication. MEMS devices are considered to range in characteristic length from one millimeter down to one micron.

MEMS sensors offer smaller size, weight and less power consumption. MEMS are capable of withstanding high non-operating shock levels, and in general offer a lower cost than other technologies. The weaknesses of MEMS inertial systems lie in critical performance parameters such as higher angle random walk/noise, which is an extremely important performance criterion in stabilization and positioning systems. Thermal sensitivity of MEMS inertial systems also impacts their bias and scale factor performance these attributes are critical in both stabilization and navigation applications [2].

## 2.4 The Mathematics Of Inertial Navigation

The complete understanding of Inertial Navigation requires a strong background on motion sensor models. Two such models (Accelerometer model and Gyroscope model) are discussed.

### 2.4.1 Accelerometer Model

Measurements from the accelerometer at the sensor frame are modelled as

$${}^s\mathbf{z}_a(k) = {}^s\mathbf{a}(k) + {}^s\mathbf{b}_a(k) + {}^s\mathbf{n}_a(k) \quad (2.1)$$

where,  $(k)$  indicates time,  ${}^s(\cdot)$  indicates that the quantity is in the sensor frame,  ${}^s\mathbf{a}(k)$  is the true acceleration vector,  ${}^s\mathbf{b}_a(k)$  is the bias in the acceleration measurement (due to gravity),  ${}^s\mathbf{n}_a(k)$  is the measurement noise which is assumed to be zero-mean white gaussian with diagonal covariance matrix. The elements of vectors  ${}^s\mathbf{z}_a(k)$ ,  ${}^s\mathbf{a}(k)$ ,  ${}^s\mathbf{b}_a(k)$  and  ${}^s\mathbf{n}_a(k)$  are given as

$$\begin{aligned} {}^s\mathbf{z}_a(k) &= \begin{bmatrix} {}^sz_{ax}(k) \\ {}^sz_{ay}(k) \\ {}^sz_{az}(k) \end{bmatrix}, & {}^s\mathbf{a}(k) &= \begin{bmatrix} {}^sa_x(k) \\ {}^sa_y(k) \\ {}^sa_z(k) \end{bmatrix}, \\ {}^s\mathbf{b}_a(k) &= \begin{bmatrix} {}^sb_{ax}(k) \\ {}^sb_{ay}(k) \\ {}^sb_{az}(k) \end{bmatrix}, & {}^s\mathbf{n}_a(k) &= \begin{bmatrix} {}^sn_{ax}(k) \\ {}^sn_{ay}(k) \\ {}^sn_{az}(k) \end{bmatrix} \end{aligned} \quad (2.2)$$

where,  ${}^s(\cdot)_x$ ,  ${}^s(\cdot)_y$ ,  ${}^s(\cdot)_z$  denotes that the quantity is in the directions  $x$ ,  $y$ , and  $z$ , respectively, of the sensor frame and the additional subscript  $(\cdot)_a$ , as in  ${}^s(\cdot)_{ax}$ ,  ${}^s(\cdot)_{ay}$ ,  ${}^s(\cdot)_{az}$ , indicates that the quantity is related to acceleration.

It is known that the bias in acceleration in the global frame is present only in the

z-direction, i.e.,

$${}^s\mathbf{b}_a(k) = \begin{bmatrix} 0 \\ 0 \\ {}^s b_{az}(k) \end{bmatrix} \quad (2.3)$$

where  ${}^s b_{az}(k) \approx -9.8 \text{ ms}^{-2}$ .

## 2.4.2 Gyroscope Model

The gyroscope measurement at the  $k^{\text{th}}$  sample is written as

$${}^s\mathbf{z}_g(k) = {}^s\boldsymbol{\psi}(k) + {}^s\mathbf{b}_g(k) + {}^s\mathbf{n}_g(k) \quad (2.4)$$

where,  ${}^s\boldsymbol{\psi}(k)$  is the true angular velocity vector,  ${}^s\mathbf{b}_g(k)$  is the bias in the gyroscope measurement,  ${}^s\mathbf{n}_g(k)$  is the measurement noise which is assumed to be zero-mean white gaussian with diagonal covariance matrix. The elements of vectors  ${}^s\mathbf{z}_g(k)$ ,  ${}^s\boldsymbol{\psi}(k)$ ,  ${}^s\mathbf{b}_g(k)$  and  ${}^s\mathbf{n}_g(k)$  are given as

$$\begin{aligned} {}^s\mathbf{z}_g(k) &= \begin{bmatrix} {}^s z_{gx}(k) \\ {}^s z_{gy}(k) \\ {}^s z_{gz}(k) \end{bmatrix}, & {}^s\boldsymbol{\psi}(k) &= \begin{bmatrix} {}^s\psi_x(k) \\ {}^s\psi_y(k) \\ {}^s\psi_z(k) \end{bmatrix}, \\ {}^s\mathbf{b}_g(k) &= \begin{bmatrix} {}^s b_{gx}(k) \\ {}^s b_{gy}(k) \\ {}^s b_{gz}(k) \end{bmatrix}, & {}^s\mathbf{n}_g(k) &= \begin{bmatrix} {}^s n_{gx}(k) \\ {}^s n_{gy}(k) \\ {}^s n_{gz}(k) \end{bmatrix} \end{aligned} \quad (2.5)$$

where,  ${}^s(\cdot)_x$ ,  ${}^s(\cdot)_y$ ,  ${}^s(\cdot)_z$  denotes that the quantity is in the directions  $x$ ,  $y$ , and  $z$ , respectively, of the sensor frame and the additional subscript  $(\cdot)_g$ , as in  ${}^s(\cdot)_{gx}$ ,  ${}^s(\cdot)_{gy}$ ,  ${}^s(\cdot)_{gz}$ , indicates that the quantity is related to gyroscope measurement, i.e., angular velocity.

## 2.5 Attitude Representation

Inertial navigation derives relative navigation parameters from a self-contained autonomous sensor system i.e. an IMU. The attitude of the IMU is determined using the measurements taken (which are in the sensor frame) and can be rotated into the global frame of reference. To accomplish this, Euler angles will be used to represent the attitude of the IMU and hence the movement of the foot itself since IMU is attached to the pedestrian's foot.

This section dedicates on describing the mathematics behind different attitude representation. Also, given that sometimes there are several different possible options for a frame to be defined (ENU: x-East, y-North, z- Up , NED: x-North, y-East ,z-Down and others), to avoid confusion, rotation around x, y ,z as roll, pitch and yaw are considered where roll is defined to be the rotation around the forward axis, while yaw us the one around the vertical axis pitch is the around the lateral axis.

### 2.5.1 Euler Angles

Euler angles are the angles of rotation of a three-dimensional coordinate frame. A rotation of Euler angles consists of three successive rotations around each one of the x-y-z axis in a sequence as addressed in equation 2.16. It is important to remark that the order in which the rotations are applied matters, given that matrix multiplication is not a commutative operation.

#### 2.5.1.1 Rotations in two dimensions

A vector in a two-dimensional space can be given either in cartesian coordinates (x, y) or in polar coordinates (r,  $\phi$ ) relative to a frame of reference as shown in figure 2.4.

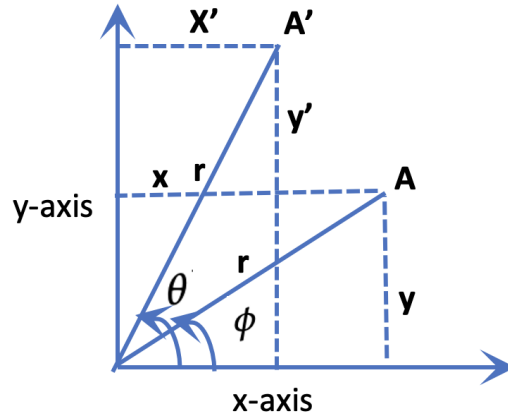


Figure 2.4: **Rotating a vector, (A).** Polar and cartesian coordinates systems.

where the formulas for transforming one representation to another is given as

$$x = r \cos \phi \quad (2.6)$$

$$y = r \sin \phi \quad (2.7)$$

$$r = \sqrt{x^2 + y^2} \quad (2.8)$$

$$\phi = \tan^{-1} \frac{y}{x} \quad (2.9)$$

Suppose now that the vector is rotated by the angle  $\theta$ . The new vector's polar coordinates are  $(r, \phi + \theta)$  and its cartesian coordinates computed using the trigonometric identities for the sum of two angles are described as follows

$$\begin{aligned} x' &= r \cos(\phi + \theta) \\ &= r(\cos \phi \cos \theta - \sin \phi \sin \theta) \\ &= (r \cos \phi) \cos \theta - (r \sin \phi) \sin \theta \\ &= x \cos \theta - y \sin \theta \end{aligned} \quad (2.10)$$

$$\begin{aligned}
y' &= r \sin(\phi + \theta) \\
&= r \sin\phi \cos\theta + \cos\phi \sin\theta \\
&= y \cos\theta + x \sin\theta \\
&= x \sin\theta + y \cos\theta
\end{aligned}
\tag{2.11}$$

The transformation of the position  $(x, y)$  to  $(x', y')$  caused by a rotation through the angle  $\theta$  can be expressed in matrix notation as [3].

$$\begin{bmatrix} x' \\ y' \end{bmatrix} = \begin{bmatrix} \cos\theta & -\sin\theta \\ \sin\theta & \cos\theta \end{bmatrix} \begin{bmatrix} x \\ y \end{bmatrix}
\tag{2.12}$$

### 2.5.1.2 Rotations in three dimensions

The concept of coordinate transformations in three-dimensions is the same as in two dimensions, however, the mathematics are more complicated. The standard x-y-z coordinate frame has the positive directions of its axes pointing in the directions (right, up, out) as described in the figure 2.5. The x-axis is drawn left and right on the paper and the y-axis is drawn up and down on the paper. The diagonal line represents the z-axis, which is perpendicular to the other two axes and therefore its positive direction is out of the paper and its negative direction is into the paper.

A three-dimensional rotation matrix will be a  $3 \times 3$  matrix because each point  $p$  in a frame has three coordinates  $p_x, p_y, p_z$  that must be moved. Consider first a rotation around the z-axis. The x and y coordinates are rotated as in two dimensions and the z coordinate remains unchanged. Therefore, the matrix would be represented

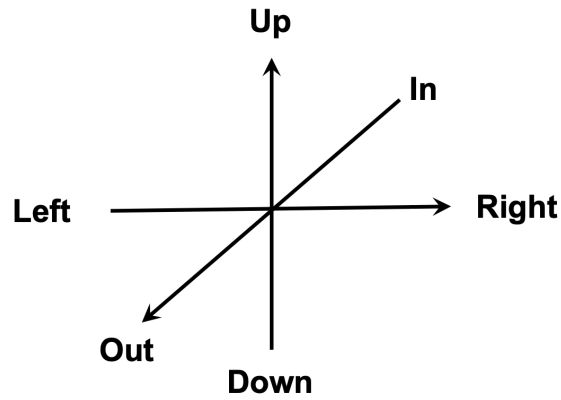


Figure 2.5: **Three-dimensional coordinate frame.** Standard x-y-z coordinate frame.

as given

$$\begin{bmatrix} \cos\theta & -\sin\theta & 0 \\ \sin\theta & \cos\theta & 0 \\ 0 & 0 & 1 \end{bmatrix} \quad (2.13)$$

For a rotation about the x-axis, the x coordinate is unchanged and the y and z coordinates are transformed “as if” they were the x and y coordinates of a rotation around the z-axis.

$$\begin{bmatrix} 1 & 0 & 0 \\ 0 & \cos\theta & -\sin\theta \\ 0 & \sin\theta & \cos\theta \end{bmatrix} \quad (2.14)$$

Similarly, for a rotation about the y-axis, the y coordinate is unchanged and the z and x coordinates are transformed “as if” they were the x and y coordinates of a

rotation around the z-axis [3].

$$\begin{bmatrix} \cos\theta & 0 & \sin\theta \\ 0 & 1 & 0 \\ -\sin\theta & 0 & \cos\theta \end{bmatrix} \quad (2.15)$$

It may seem strange that the signs of  $\sin \theta$  have changed. Instead of performing the three multiplications of a vector by a matrix, we can multiply the matrices for the three Euler angles together using Equation 2.16.

The greatest advantage of this particular order is that it keeps the heading constant regardless to roll and pitch applied, therefore explaining its wide use in marine and air traffic control. Though Euler angles are limited by a phenomenon called "gimbal lock," which prevents them from measuring orientation when the pitch angle approaches +/- 90 degrees. Quaternions provide an alternative measurement technique which does not suffer from gimbal lock also quaternions are less intuitive than Euler angles and the math can be a little more complicated.

## 2.5.2 Quaternions

Quaternions are an algebraic structure that extends the familiar concept of complex numbers. While quaternions are much less intuitive than angles, rotations defined by quaternions can be computed more efficiently and with more stability, and therefore are widely used applications which requires precise orientation response.

This dissertation is limited to use of three-dimensional Euler angles for recursive orientation estimates.

## 2.6 Coordinate Systems and Transformations

Inertial navigation system requires transformation of measured and computed quantities between various frames of reference. In the scope of this thesis there are two

frames, the global frame (g-frame) which is the navigation frame and the sensor frame (s-frame) which is the frame used by IMU. Our system uses the standard strapdown inertial navigation system mechanization. The INS navigation is performed relative to the fixed sensor frame. Typically, this integration needs following stages [4].

- The accelerometer and the gyro use the s-frame inside the IMU. First the heading information is updated with integration of the measured angular rates from the s-frame. Then the coordinate transformation matrix is calculated.
- The g-frame accelerations are transformed to calculate the g-frame accelerations and angular velocity by using the transformation matrix.
- The g-frame accelerations are integrated to calculate the g-frame velocity and position.

The relationship between the coordinate frames is given by the coordinate rotation matrix which is a  $3 \times 3$  matrix. In this chapter some of the necessary coordinate frames for the thesis are defined and the derivation necessary to transform between the reference frames are presented.

### **2.6.1 Sensor Frame (s-frame)**

The sensor frame is sometime called vehicle frame. In our navigation application, the objectives is to determine the position of the user based on the measurements from the sensor platform attached to the user, see Figure 2.3 The sensor frame is rigidly attached to the user's boot. The x-axis is defined in the forward direction, the z-axis is defined to pointing to the bottom of the user's foot and y-axis completes the right-handed orthogonal coordinate system.

## 2.6.2 Global Frame (g-frame)

The global plane is also called local geodetic plane. The global plane has the Euler angle i.e. pitch, roll and yaw. The global plane is attached to a fixed point on the surface of the earth at some convenient point for local measurements. This point is the origin of the local frame. The x-axis points roll, y-axis pitch east and the z-yaw completes the right-handed coordinate system pointing toward that interior of the earth perpendicular to the reference ellipsoid. The global plane is the navigation frame in this thesis work.

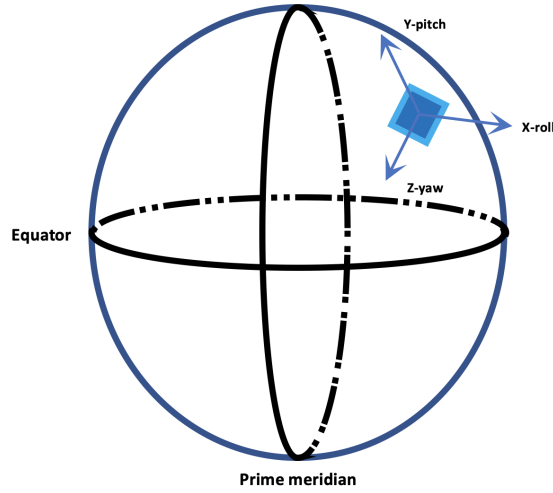


Figure 2.6: Global frame reference coordinate system. g-frame.

$$\Theta(k) = \begin{bmatrix} c(\alpha(k))c(\beta(k)) & c(\alpha(k))s(\beta(k))s(\gamma(k)) - s(\alpha(k))c(\gamma(k)) & c(\alpha(k))s(\beta(k))c(\gamma(k)) + s(\alpha(k))s(\gamma(k)) \\ s(\alpha(k))c(\beta(k)) & s(\alpha(k))s(\beta(k))s(\gamma(k)) + c(\alpha(k))c(\gamma(k)) & s(\alpha(k))s(\beta(k))s(\gamma(k)) - c(\alpha(k))s(\gamma(k)) \\ -s(\beta(k)) & c(\beta(k))s(\gamma(k)) & c(\beta(k))c(\gamma(k)) \end{bmatrix} \quad (2.16)$$

where

$$\begin{aligned} \alpha(k) &= \text{Yaw}, \beta(k) = \text{Pitch}, \gamma(k) = \text{Roll}, \\ c(\alpha(k)) &= \cos(\alpha(k)), c(\beta(k)) = \cos(\beta(k)), c(\gamma(k)) = \cos(\gamma(k)), \\ s(\alpha(k)) &= \sin(\alpha(k)), s(\beta(k)) = \sin(\beta(k)), s(\gamma(k)) = \sin(\gamma(k)). \end{aligned}$$

### 2.6.3 Coordinate Frame Transformation

In order to track the movement of the object in a *global frame*, the acceleration measurements in (2.1) needs to be converted to global frame. This is achieved through the premultiplication of the *rotation matrix*  $\Theta(k)$ , given in (2.16), i.e.,

$${}^g\mathbf{z}_a(k) = \Theta(k) {}^s\mathbf{z}_a(k) \quad (2.17)$$

where  ${}^s\mathbf{z}_a(k)$  is the accelerometer measurement in the sensor frame and  ${}^g\mathbf{z}_a(k)$  is the accelerometer measurement that is converted to the global frame.

Now, let us substitute for  $\mathbf{z}_a(k)$  in (2.17) from (2.1)

$${}^g\mathbf{z}_a(k) = \Theta(k) {}^s\mathbf{a}(k) + \underbrace{\Theta(k) {}^s\mathbf{b}_a(k)}_{= {}^g\mathbf{b}_a(k)} + \Theta(k) {}^s\mathbf{n}_a(k) \quad (2.18)$$

$${}^g\mathbf{z}_a(k) - {}^g\mathbf{b}_a(k) = {}^g\mathbf{a}(k) + {}^g\mathbf{n}_a(k) \quad (2.19)$$

$$\mathbf{z}_a(k) = \mathbf{a}(k) + \mathbf{n}_a(k) \quad (2.20)$$

where  $\mathbf{z}_a(k)$  is the *gravity adjusted measurement* of the acceleration in the global frame.

The rotation matrix defined in (2.16) makes use of the rotation angles about the  $z$ ,  $y$  and  $x$ -axis respectively at time  $k$ , defined respectively as, yaw  $\alpha(k)$ , pitch  $\beta(k)$ , and roll  $\gamma(k)$ .

$$\alpha(k) = 0 \quad (2.21)$$

$$\beta(k) = -\tan^{-1} \left( \frac{{}^s a_x(k)}{{}^s a_z(k)} \right) \quad (2.22)$$

$$\gamma(k) = \tan^{-1} \left( \frac{{}^s a_y(k)}{{}^s a_z(k)} \right) \quad (2.23)$$

Initially we start by computing yaw, pitch and roll as described through equations (2.21-2.23) this in turn is used to calculate rotation matrix using Euler's angle as

described in equation (2.16).

The skew-symmetric angular rate matrix  $\mathbf{\Omega}(k)$  formed by the gyroscope readings along  $x, y$  and  $z$  direction respectively.

$$\mathbf{\Omega}(k) = \begin{bmatrix} 0 & -{}^s\psi_z(k) & {}^s\psi_y(k) \\ {}^s\psi_z(k) & 0 & -{}^s\psi_x(k) \\ -{}^s\psi_y(k) & {}^s\psi_x(k) & 0 \end{bmatrix} \quad (2.24)$$

The rotation matrix along with the skew-symmetric angular rate matrix is used to calculate the orientation  $\mathbf{\Theta}(k)$  along  $x, y$  and  $z$  direction respectively.

$$\mathbf{\Theta}(k) = \mathbf{\Theta}(k-1)(2\mathbf{I}_3 + \mathbf{\Omega}(k)\Delta(k))(2\mathbf{I}_3 - \mathbf{\Omega}(k)\Delta(k))^{-1} \quad (2.25)$$

by using the above equation (2.25) we iteratively update the orientation using the previous estimate of rotation matrix and the obtained skew-symmetric angular rate matrix where  $\Delta_k$  is the time step [?].

Transforming the acceleration to global frame using the above obtained orientation matrix. We then integrate the acceleration in the global frame minus gravity to obtain the velocity estimate.

$${}^g\mathbf{a}(k) = (\mathbf{\Theta}(k) + {}^{gs}\mathbf{\Theta}(k-1)){}^s\mathbf{a}(k)/2 \quad (2.26)$$

$$\mathbf{v}(k) = \mathbf{v}(k-1) + \frac{1}{2}({}^g\mathbf{a}(k) + {}^g\mathbf{a}(k-1)) - 2{}^g\mathbf{b}_a(k)\Delta(k) \quad (2.27)$$

Computing the Position in global frame. The position estimate is computed by integrating the velocity.

$$\boldsymbol{\omega}(k) = \boldsymbol{\omega}(k-1) + \frac{1}{2}(\mathbf{v}(k) + \mathbf{v}(k-1))\Delta(k) \quad (2.28)$$

## 2.7 Correcting Inertial Navigation

The observations that an IMU provides are contaminated with both stochastic and systematic errors. Environmental factors and processing requirements are also among the main sources of error when estimating position from IMU data. The accuracy of any navigation system is directly related to the mitigation of these errors and therefore identification of the errors in an observation equation is critical for better state estimation.

### 2.7.1 Error Types: MEMS Accelerometers and Gyroscopes Sources of Error

Accelerometer and gyroscope errors typically include biases, scale factors, triad non-orthogonality and noise. The magnitude of the noise and the stability of biases are the two common attributes that usually determine the quality of the sensor. The quality of an IMU is typically reflected in its cost [5].

- **Bias:** The bias of an inertial system is the average output from the sensor when it is not undergoing any rotation (i.e: the offset of the output from the true value), in  $h$ .
- **Thermo-Mechanical White Noise:** The output samples obtained from a MEMS accelerometer are perturbed by a white noise sequence.
- **Bias Stability:** MEMS accelerometers are subject to flicker noise, which causes the bias to wander over time. Such fluctuations are usually modelled as a bias random walk.
- **Temperature Effects:** As with any type of passive sensors, temperature changes cause fluctuations in the bias of the output signal. The relationship between bias and temperature depends on the specific device, however it is often highly nonlinear. Any residual bias introduced causes an error in position which grows

quadratically with time, If the IMU contains a temperature sensor then it is possible to apply corrections to the output signals in order to compensate for temperature dependent effects.

- Calibration Errors: Calibration errors (errors in scale factors, alignments and output linearities) appear as bias errors which are only visible whilst the device is undergoing acceleration. Note that these ‘temporary’ bias errors may be observed even when the device is stationary due to gravitational acceleration.

Table 2.1 and Table 2.2 summarizes the types of errors encountered in accelerometer and gyroscope respectively [5].

Table 2.1: Accelerometer Error Sources

Error Type	Description	Result of Double Integration
Bias	A constant bias $\epsilon$ in the accelerometer’s output signal	A quadratically growing position error ${}^s\mathbf{b}_a(k) = \epsilon \frac{t^2}{2}$
White Noise	White noise with some standard deviation $\sigma$	A second-order random walk. The standard deviation of the position error grows as ${}^s\mathbf{n}_a(k) = \sigma t^{3/2} \sqrt{\frac{\delta t}{3}}$
Temperature Effects	Temperature dependent residual bias	Any residual bias causes an error in position which grows quadratically with time
Calibration	Deterministic errors in scale factors, alignments and accelerometer linearities	Position drift proportional to the squared rate and duration of acceleration
Bias Instability	Bias fluctuations, usually modelled as a bias random walk	A third-order random walk in position

## 2.7.2 Environmental Influences on Quality of Data Collected

Structural elements of buildings (i.e. ferrous metals, elevators, etc.) influence IMU data and orientation estimation. Results found that changes in environment (rural vs clinical) did not affect the static accelerometer and magnetometer data, but changes to location within a building did affect both magnetometer and accelerometer data.

Table 2.2: Gyroscope Error Sources

Error Type	Description	Result of Double Integration
Bias	A constant bias $\epsilon$	A steadily growing angular error ${}^s\mathbf{b}_g(k) = \epsilon t$
White Noise	White noise with some standard deviation $\sigma$	An angle random walk, whose standard deviation ${}^s\mathbf{n}_g(k) = \sigma \sqrt{\delta t \times t}$ grows with the square root of time
Temperature Effects	Temperature dependent residual bias	Any residual bias is integrated into the orientation, causing an orientation error which grows linearly with time
Calibration	Deterministic errors in scale factors, alignments and gyroscope linearities	Orientation drift proportional to the rate and duration of motion
Bias Instability	Bias fluctuations, usually modelled as a bias random walk	A second-order random walk

Ferrous metals, often used in building materials, can affect data acquisition by a magnetometer in a clinical setting [6]. Using six-degrees of freedom boycotts the influence of magnetometer data and relies on the accuracy of acquired acceleration and rate gyroscope data to predict the next iteration of the dataset. Careful setup needs to be attended to when securing IMU devices to align with anatomical reference frames and the development of inertial reference frames needs special consideration due to the errors that can occur with local frame data acquisition.

## 2.8 Bibliography

- [1] C. L. Vaughan, “Theories of bipedal walking: an odyssey,” *Journal of biomechanics*, 2003. pages 15, 16
- [2] Y. Dong, P. Zwahlen, A. Nguyen, R. Frosio, and F. Rudolf, “Ultra-high precision mems accelerometer,” in *2011 16th International Solid-State Sensors, Actuators and Microsystems Conference*, 2011. pages 18
- [3] M. Ben-Ari, “A tutorial on euler angles and quaternions,” *Weizmann Institute of Science, Israel*, 2014. pages 23, 25
- [4] S. Rajagopal, “Personal dead reckoning system with shoe mounted inertial sensors,” *Master’s Degree Project, Stockholm, Sweden*, 2008. pages 26
- [5] O. J. Woodman, “An introduction to inertial navigation,” tech. rep., 2007. pages 30, 31
- [6] W. De Vries, H. Veeger, C. Baten, and F. Van Der Helm, “Magnetic distortion in motion labs, implications for validating inertial magnetic sensors,” *Gait & posture*, 2009. pages 32

## Chapter 3

# THEORY OF ADAPTIVE ESTIMATION

### 3.1 Calibration

Calibration is very important step to determine the accuracy of the instrument and to ensure the readings are consistent through the measurements. The calibration has to be done every time for a low-cost sensor, these calibration values are rough because it would be too expensive to calibrate well, for an inexpensive sensor. On the other hand, manufacturer will provide the factory values for industrial grade inertial sensors which represent the corrected scaling values. As inertial sensors are sensitive to temperature changes the process of understanding the variation of these errors at different temperature points is an important step for improving performance of inertial sensors and hence the performance of navigation system [1]. Thus, in this work, it is assumed that the temperature remains constant during the entire duration of the experiment.

## 3.2 The Kalman Filter (KF)

The Kalman filter is a set of mathematical equations that implement a predictor-corrector type estimator that is optimal in the sense that it minimizes the estimated error covariance. The KF has been the subject of extensive research and application, particularly in the area of autonomous or assisted navigation. This may be accounted to the advancement in digital computing that made the use of the filter practical, but also to the relative simplicity and robust nature of the filter itself. Rarely do the conditions necessary for optimality actually exist, and yet the filter apparently works well for many applications in spite of this situation.

Kalman filter is well known for its good performance to remove gaussian noise also Kalman filter is a model-based filter, which means a correct model is important to get the good filtering results.

### 3.2.1 The Standard Kalman Filtering Algorithm

Kalman filter is described by the following state space equations. It addresses the general problem of trying to estimate the state  $\mathbf{x} \in \mathbb{R}^n$  of a discrete-time controlled process that is governed by the linear stochastic difference equation with a measurement  $\mathbf{y} \in \mathbb{R}^m$ .

$$\mathbf{x}(k) = \mathbf{A}\mathbf{x}(k-1) + \mathbf{B}\mathbf{u}(k-1) + \mathbf{v}(k) \quad (3.29)$$

$$\mathbf{y}(k) = \mathbf{C}\mathbf{x}(k) + \mathbf{w}(k) \quad (3.30)$$

The process equation given in the following equation (3.29) is assumed to be linear with respect to the state estimate. Where, the state and input vector is given by  $\mathbf{x}(k)$  and  $\mathbf{u}(k)$ . The state transition matrix and the control variable matrix are represented as  $\mathbf{A}$  and  $\mathbf{B}$ . The system process noise  $\mathbf{v}(k)$  is assumed to be zero-mean

white Gaussian noise.

The measurement equation is as shown in equation (3.30). Where,  $\mathbf{C}(k)$  is the measurement matrix,  $\mathbf{y}(k)$  is the measurement quantity used to update the state estimate, and  $\mathbf{w}(k)$  is the measurement noise assumed to be zero-mean white Gaussian noise. The process noise and the measurement noise of the state space equation (3.29)-(3.30) are represented as shown below.

$$\mathbf{v}(k) = [v_1(k), v_2(k), \dots, v_n(k)]^T \quad (3.31)$$

$$\mathbf{w}(k) = [w_1(k), w_2(k), \dots, w_m(k)]^T \quad (3.32)$$

where, the process noise covariance  $\mathbf{Q}$  and measurement noise covariance  $\mathbf{R}$  are depicted as.

$$E \{ \mathbf{v}(k) \mathbf{v}(k)^T \} = \mathbf{Q} \quad (3.33)$$

$$E \{ \mathbf{w}(k) \mathbf{w}(k)^T \} = \mathbf{R} \quad (3.34)$$

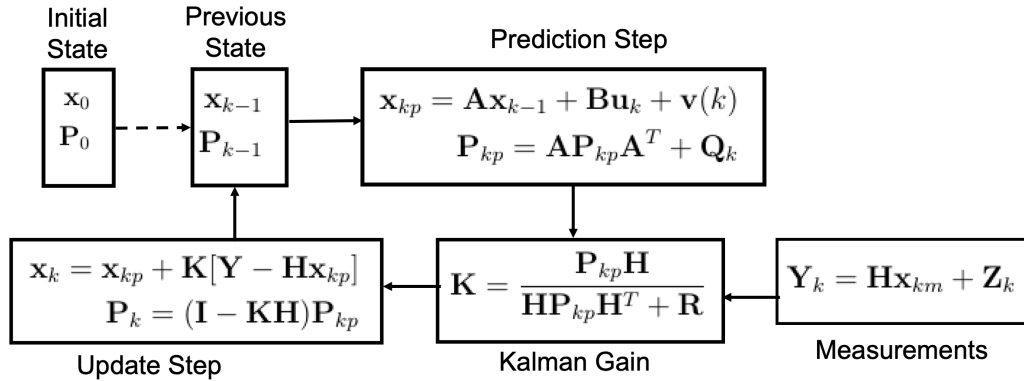


Figure 3.7: **Kalman filter Algorithm A** block diagram of the KF algorithm.

Kalman Filter is an iterative mathematical process that uses a set of equations and consecutive data inputs to quickly estimate the true states (position, velocity etc..) of the object being measured,

when the measured values contain unpredicted or random error, uncertainty or variation.

---

**Algorithm 1 :One iteration of Kalman filter**

---

$$[\hat{\mathbf{x}}(k|k), \hat{\mathbf{P}}(k|k)] = \text{KF}(\mathbf{x}(k-1|k-1), \mathbf{P}(k-1|k-1), \mathbf{y}(k))$$


---

- 1: State prediction:  $\hat{\mathbf{x}}(k|k-1) = \mathbf{A}(k)\hat{\mathbf{x}}(k-1|k-1) + \mathbf{B}(k)\mathbf{u}(k)$
  - 2: State prediction Cov:  $\mathbf{P}(k|k-1) = \mathbf{A}(k)\mathbf{P}(k-1|k-1)\mathbf{A}(k)^T + \mathbf{Q}$
  - 3: Innovation Cov:  $\mathbf{S}(k) = \mathbf{C}(k)\mathbf{P}(k|k-1)\mathbf{C}(k)^T + \mathbf{R}$
  - 4: Measurement prediction:  $\hat{\mathbf{y}}(k|k-1) = \mathbf{C}(k)\hat{\mathbf{x}}(k|k-1)$
  - 5: Measurement Residual:  $\boldsymbol{\nu}(k) = \mathbf{y}(k) - \hat{\mathbf{y}}(k|k-1)$
  - 6: Filter Gain:  $\mathbf{K}(k) = \mathbf{P}(k|k-1)\mathbf{C}(k)^T\mathbf{S}(k)^{-1}$
  - 7: State Est:  $\hat{\mathbf{x}}(k|k) = \hat{\mathbf{x}}(k|k-1) + \mathbf{K}(k)\boldsymbol{\nu}(k|k-1)$
  - 8: State Est. Cov:  $\mathbf{P}(k|k) = (\mathbf{I} - \mathbf{K}(k)\mathbf{C}(k))\mathbf{P}(k|k-1)$
- 

### 3.2.2 Implementing Kalman Filter

Figure 3.8 represents two automobiles: vehicle A and B where the objective of vehicle A is to continuously measures the distance between the vehicle B and itself with the help of radar mounted on a front-bumper. Based on the estimated distance, the vehicle adjusts its controls to maintain a constant distance (Similar to a cruise control vehicle on a highway). Main challenges encountered are the noisy radar measurements  $z(k)$ . The point of interest is finding the distance  $x(k)$  to vehicle B where velocity  $\dot{x}(k)$  and acceleration  $\ddot{x}(k)$  are also of our interest?

Approach used is Kalman filter to recursively estimate the state (position, velocity and acceleration) of the vehicle B. We Assume that the radar measurements are taken at a sampling rate of 10 Hz and simulate 100 measurement samples, i.e,  $k = 1, 2, \dots, 100$ , with the following assumptions that initial state is zero vector, i.e.  $x(0) = [0, 0, 0]^T$ . The vehicle starts from rest with a processing noise  $\tilde{q}$  equal to 0.001.

The true position and velocity and observations for a run of 100 samples computed from the system equations using a pseudo-random number generator to generate normally distributed random numbers for the variances  $\sigma_q^2, \sigma_r^2$ .

The process model of the vehicle and the measurement model obtained by the radar can be modelled as

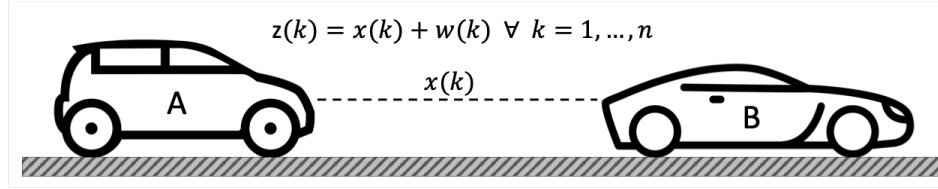


Figure 3.8: **Recursively estimating the state of vehicle B with respect to vehicle A.** Using Kalman filtering Algorithm.

$$\mathbf{x}(k+1) = \mathbf{A}\mathbf{x}(k) + \mathbf{v}(k) \quad (3.35)$$

$$\begin{bmatrix} x(k+1) \\ \dot{x}(k+1) \\ \ddot{x}(k+1) \end{bmatrix} = \begin{bmatrix} 1 & \Delta t & \Delta t^2/2 \\ 0 & 1 & \Delta t \\ 0 & 0 & 1 \end{bmatrix} \begin{bmatrix} x(k) \\ \dot{x}(k) \\ \ddot{x}(k) \end{bmatrix} + \begin{bmatrix} v_1(k) \\ v_2(k) \\ v_3(k) \end{bmatrix} \quad (3.36)$$

$$z(k) = \mathbf{C}\mathbf{x}(k) + w(k) \quad (3.37)$$

$$z(k) = \begin{bmatrix} 1 & 0 & 0 \end{bmatrix} \begin{bmatrix} x(k) \\ \dot{x}(k) \\ \ddot{x}(k) \end{bmatrix} + w(k) \quad (3.38)$$

### 3.2.3 Performance Analysis

In this section we consider how to evaluate the performance of a Kalman filter. We analysis the performance by comparing the true, measured and estimated state along with their error covariance measurement. Since in practice we cannot measure performance with respect to the state error measures (since we don't know the true state values) how do we check that the filter is performing correctly? The answer is that we can define filter performance measures in terms of the innovation. Under the hypothesis that the filter is consistent, the normalised innovations squared  $\chi^2$  Test

(NIS).

$$\epsilon(k) = \boldsymbol{\nu}(k)' \mathbf{S}(k)^{-1} \boldsymbol{\nu}(k) \quad (3.39)$$

has a chi-square distribution with  $n$  degree of freedom, where  $n$  is the measurement of dimension of the measurement.

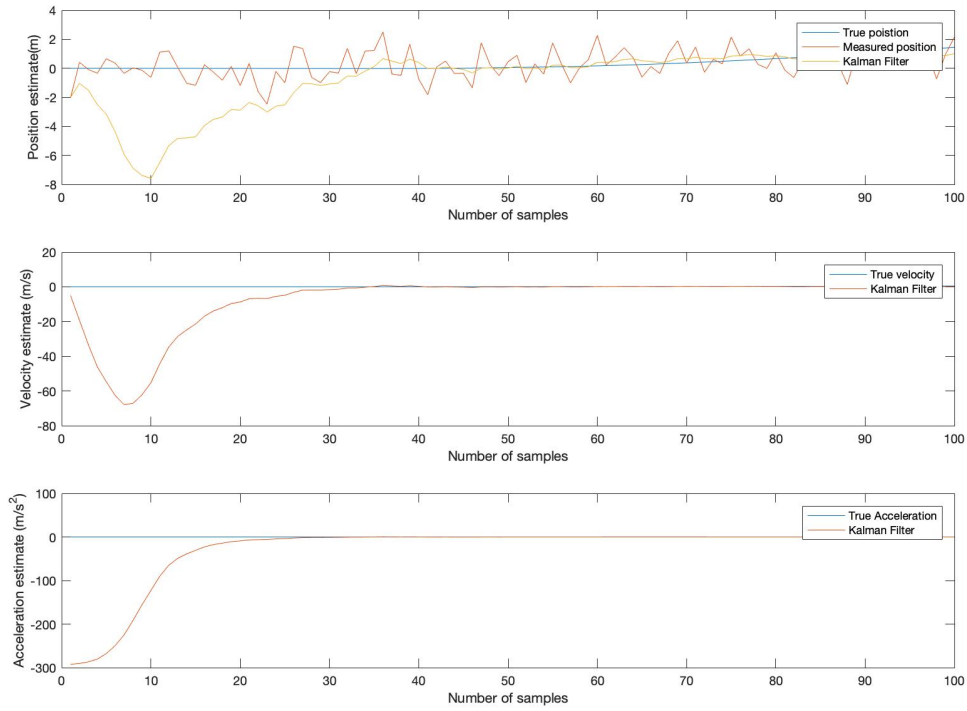


Figure 3.9: **States of vehicle B are plotted.** (a) True position, measured position and estimated position (KF) (b) True velocity, estimated velocity (KF) and (c) True acceleration, estimated acceleration (KF).

### 3.2.4 Conclusion

Figure 3.9 shows the tracking results achieved by applying the Kalman filter algorithm where figure 3.9(a) shows the the true, measured and estimated position. Similarly figure 3.9(b) and 3.9(c) shows the relation between velocity and acceleration (true

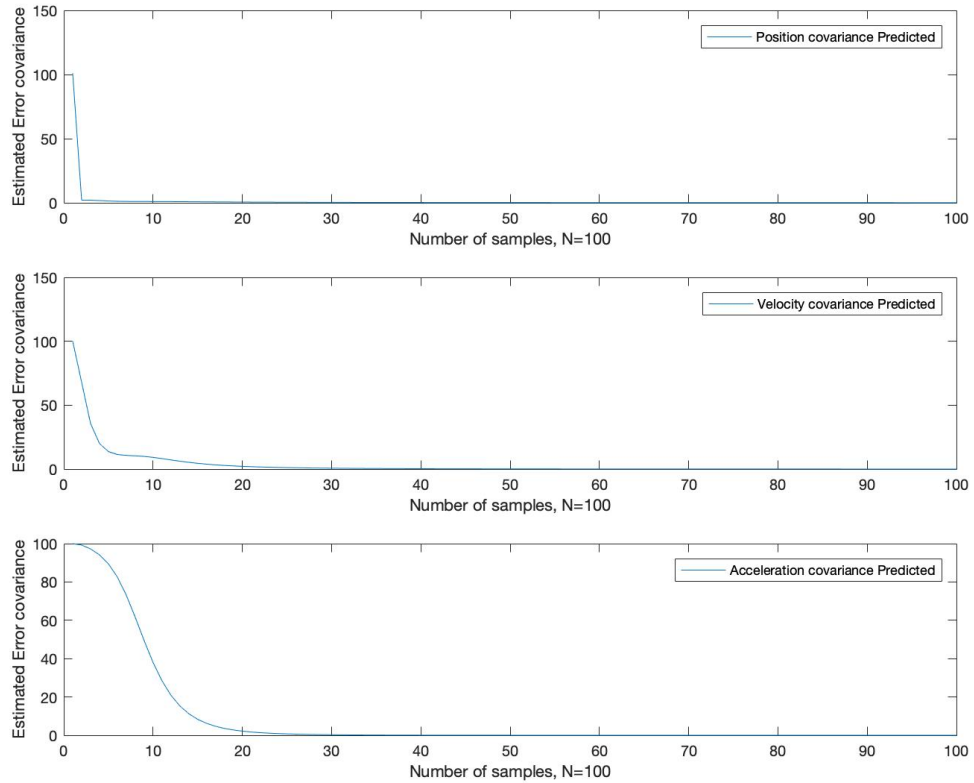


Figure 3.10: **Estimating the error covariance of vehicle B.** (a) Position error covariance (b) Velocity error covariance and (c) Acceleration error covariance.

and estimated) of the system. This follows from the fact that the update is a weighted sum of the predicted and measured. As  $k$  increases the steady state is achieved.

The error covariance reported by an estimation is said to be consistent if it is a reliable indicator of the actual error. Figure 3.10 shows the estimated error covariance for position, velocity and acceleration. In particular, note that they all tend to a constant value as  $k$  gets larger. i.e. performance turns to be dependent on the values chosen for the process and measurement noise covariance matrices,  $Q$  and  $R$ .

Figure 3.11 represents the normalised innovations squared where it has a chi-square distribution with 3 degree of freedom. From  $k$  independent samples the calculated average NIS is 1.156 ( $\chi_3^2 = 1.156$ ) therefore the probability of the normal

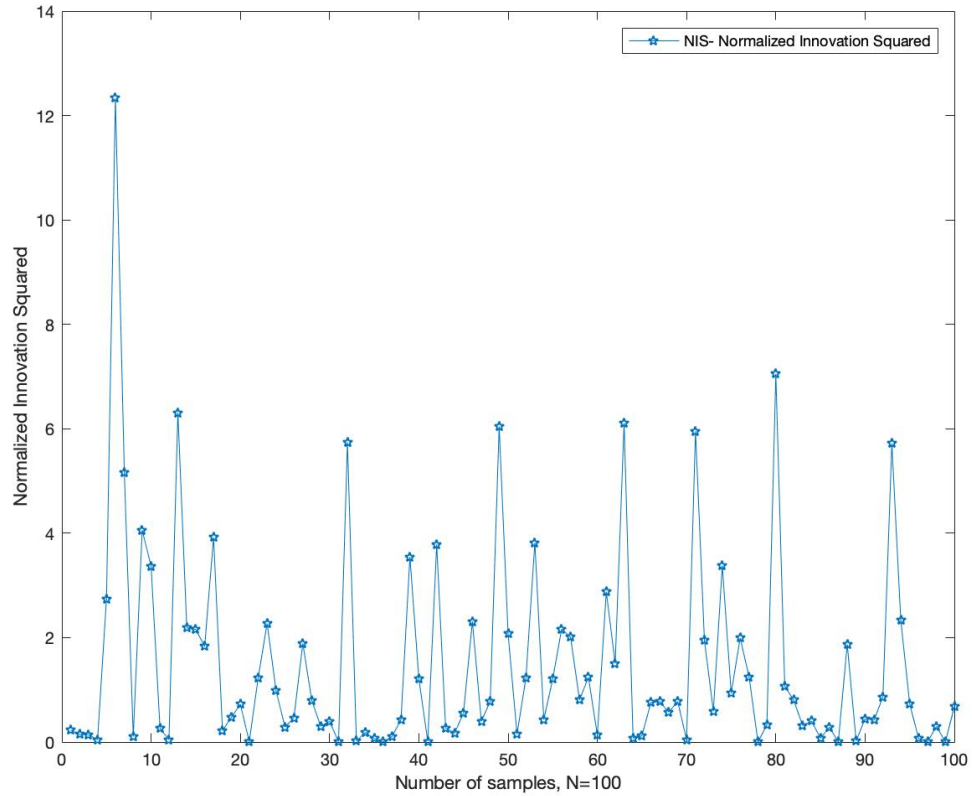


Figure 3.11: **Normalised Innovations Squared (NIS)** Used to check the consistency of Kalman filter.

distribution falls in the range of (0.5-0.75) from the Chi-Square Probabilities table.

also, so far we have only considered the performance of a Kalman filter when both the system model and noise processes are known precisely. A Kalman filter may not perform correctly if there is either modelling or noise estimation error or both.

### 3.3 Interactive Multiple Model (IMM)

Accurate state estimation of targets with changing dynamics can be achieved through the use of multiple filter model. The IMM algorithm provides a structure to efficiently

manage multiple filter models. Two important requirements for design of IMM algorithm are described as [1].

- Selection of the number and type of filter models.
- Selection of each of the individual filters parameters.

### 3.3.1 The Standard Interactive Multiple Model (IMM) Algorithm

The IMM algorithm is a method for combining state hypotheses from multiple filter models to get a better state estimate of targets with changing dynamics. The filter models used in IMM for each state hypothesis can be selected to match the behaviour of targets of interest. Model management for the IMM algorithm is governed by an underlying Markov chain that controls the switching behaviour among the multiple models.

Multiple filter models (hybrid system) enable a tracking system to better match changing targets dynamics. This will yield the best overall performance on both maneuvering and non-maneuvering time intervals of targets. The Observed system is assumed to evolve according to one out of  $r$  possible linear gaussian models which jumps between these models according to a Markov chain. The conditional probability density function (pdf) of the state  $x$  is decomposed according to the total probability theorem as follows [2, 3].

$$\begin{aligned}
 p[x(k)|Z^k] &= \sum_{j=1}^r p[x(k)|M_j(k), Z^k]P\{M_j(k)|Z^k\} \\
 &\triangleq \sum_{j=1}^r p[x(k)|M_j(k), z^k, Z^{k-1}]\mu_j(k)
 \end{aligned}
 \tag{3.40}$$

i.e,  $r$  filters are running in parallel. The notation  $M_j(k)$  stands for model  $j$  in effect during the period ending at time  $k$  and  $z^k$  is the cumulative data at  $k$ .

The model-conditioned posterior pdf of the state, is given by

$$\begin{aligned}
p[x(k)|M_j(k), z(k), Z^{k-1}] &= \frac{p[z(k)|M_j(k), x(k)]}{p[z(k)|M_j(k), Z^{k-1}]} \\
&\times p[x(k)|M_j(k), Z^{k-1}]
\end{aligned} \tag{3.41}$$

reflects the update step of the state estimation filter matched to  $M_j(k)$ . The total probability theorem is now applied to the last term above (the prior), yielding

$$\begin{aligned}
p[x(k)|M_j(k), z(k), Z^{k-1}] &= \sum_{i=1}^r p[x(k)|M_j(k), M_i(k-1), Z^{k-1}] \\
&\times P\{M_i(k-1)|M_j(k), Z^{k-1}\} \\
&\approx \sum_{i=1}^r p[x(k)|M_j(k), M_i(k-1), \{\hat{x}^1(k-1|k-1), \\
&\times P^1(k-1|k-1)_{l=1}^r\} \mu_{i|j}(k-1)(k-1)] \\
&= \sum_{i=1}^r p[x(k)|M_j(k), M_i(k-1), \hat{x}^1(k-1|k-1), \\
&\times P^i(k-1|k-1)_{l=1}^r\} \mu_{i|j}(k-1)(k-1)
\end{aligned} \tag{3.42}$$

The second line above reflects the approximation that the past through  $k-1$  is summarized by  $r$  model-conditioned estimates and covariances. The last line of (3.42) is a mixture with weightings, denoted as  $\mu_{i|j}(k-1|k-1)$ , different for each current model  $m_j(k)$ . This mixture is assumed to be a mixture of Gaussian pdfs (a Gaussian sum) and then approximated via moment matching by a single Gaussian:

$$\begin{aligned}
p[x(k)|M_j(k), Z^{k-1}] &= \sum_{i=1}^r \mathcal{N}[x(k); E[x(k)|M_j(k), \hat{x}^i(k-1|k-1)], cov[.]] \\
&\times \mu_{i|j}(k-1|k-1) \\
&\approx [x(k); \sum_{i=1}^r E[x(k)|M_j(k), \hat{x}^i(k-1|k-1)] \\
&\times \mu_{i|j}(k-1|k-1), cov[.]] \\
&= [x(k); E[x(k)|M_j(k), \sum_{i=1}^r \hat{x}^i(k-1|k-1)] \\
&\times \mu_{i|j}(k-1|k-1)], cov[.]
\end{aligned} \tag{3.43}$$

where the notation  $n[x; \bar{x}; P]$  stands for the Gaussian pdf with argument  $x$ , mean  $\bar{x}$ , and covariance  $P$ . The last line above follows from the linearity of the Kalman filter and shows that the input to the filter matched to model  $j$  is obtained from an interaction of the  $r$  filters, which consists of the mixing of the estimates  $\hat{x}^i(k-1|k-1)$  according to the weightings (probabilities)  $\mu_{i|j}(k-1|k-1)$ . These steps are equivalent to hypothesis merging at the beginning of the cycle of model conditioned (Kalman) filtering.

Figure illustrates this algorithm, which consists of  $r$  interacting filters operating in parallel. The mixing is done at the input of the filter with the probabilities, detailed later, conditioned on  $z^{(k-1)}$ .

One cycle of the algorithm consists of the following.

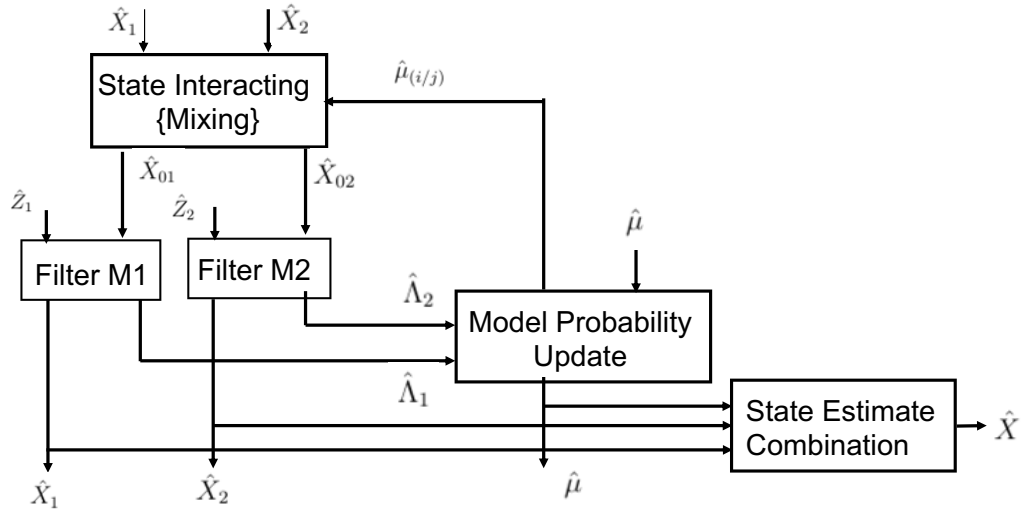


Figure 3.12: **Interactive Multiple Model Algorithm.** A block diagram of the IMM algorithm with two filter models.

### 3.3.1.1 State Interaction

Starting with  $\hat{x}^i(k-1|k-1)$  one computes the mixed initial condition for the filter matched to  $m_j(K)$  according to (4) as follows

$$\hat{x}^{0i}(k-1|k-1) = \sum_{i=1}^r \hat{x}^i(k-1|k-1) \mu_{i|j}(k-1|k-1) \quad (3.44)$$

Where

$$\begin{aligned} \mu_{i|j}(k-1|k-1) &\triangleq P\{M_i(k-1)|M_j(k), Z^{k-1}\} \\ &= \frac{1}{\bar{c}_j} P\{M_j(k)|M_i(k-1), Z^{k-1}\} P\{M_i(k-1)|Z^{k-1}\} \\ &= \frac{1}{\bar{c}_j} p_{ij} \mu_i(k-1) \end{aligned} \quad (3.45)$$

In the above,  $p_{ij}$  is the assumed transition probability for the Markov chain according to which the system model switches from model  $i$  to model  $j$ , and  $\bar{c}_j$  is the normalized constant.

The covariance corresponding to (3.44) is, according to the mixture moment-matching equations.

$$\begin{aligned}
P^{0j}(k-1|k-1) &= \sum_{i=1}^r \mu_{ij}(k-1|k-1) \{P^i(k-1|k-1) \\
&\quad + [\hat{x}^i(k-1|k-1) - \hat{x}^{0j}(k-1|k-1)] \\
&\quad \times [\hat{x}^i(k-1|k-1) - \hat{x}^{0j}(k-1|k-1)]^T\}
\end{aligned} \tag{3.46}$$

The estimate (3.44) and covariance (3.46) are used as input to the Kalman filter matched to  $M_j(k)$  to yield  $\hat{x}^j(k|k)$  and  $P^j(k|k)$ .

The likelihood functions corresponding to the  $r$  filters are computed according to

$$\begin{aligned}
\Lambda_j(k) &= p[z(k)|M_j(k), Z^{k-1}] \\
&= p[z(k)|M_j(k), \hat{x}^{0j}(k-1|k-1), p^{0j}(k-1|k-1)]
\end{aligned} \tag{3.47}$$

### 3.3.1.2 Model Probability Update

The model probabilities are updated as follows:

$$\begin{aligned}
\mu_j(k) &\triangleq P\{M_j(k)|Z^k\} \\
&= \frac{1}{c} p[z(k)|M_j(k), Z^{k-1}] P\{M_j(k)|Z^{k-1}\} \\
&= \frac{1}{c} \Lambda_j(k) \sum_{i=1}^r P[M_j(k)|M_i(k-1), Z^{k-1}] \\
&\quad \times P\{M_i(k-1)|Z^{k-1}\} \\
&= \frac{1}{c} \Lambda_j(k) \sum_{i=1}^r p_{ij} \mu_i(k-1) = \frac{1}{c} \Lambda_j(k) \bar{c}_j
\end{aligned} \tag{3.48}$$

where  $\bar{c}_j$  is the normalized constant from (3.45).

### 3.3.1.3 State Estimate Combination

Finally, for output only, the latest state estimate and covariance are obtained in view of (3.40), according to the mixture equation, as follows

$$\hat{x}(k|k) = \sum_{j=1}^r \hat{x}^j(k|k) \mu_j(k) \quad (3.49)$$

$$P(k|k) = \sum_{j=1}^r \mu_j(k) \{ P^j(k|k) + [\hat{x}^j(k|k) - \hat{x}(k|k)] \times [\hat{x}^j(k|k) - \hat{x}(k|k)]^T \} \quad (3.50)$$

## 3.3.2 Implementing Interactive Multiple Model (IMM)

The performance of many human tracking algorithms relies on accurate motion models. Due to the nature of human motion it is often difficult to determine the suitability of a chosen model. It is typically the case that over the tracking duration the characteristics of the observed motion will fit many different models. Commonly used motion models in the area of tracking include the constant velocity (CV), constant acceleration (CA) and co-ordinated turn motion models (CT).

Three filter models have been selected to test the IMM algorithm with different configurations. These models are a CV, CA and CT. As we can see from results presented in previous subsections, if we have ideal a priori knowledge and have a suitable system model, we can have rather desirable estimates on the state.

### 3.3.2.1 Constant Velocity (CV)

If we have a priori knowledge that the vehicle moves at constant velocity, we may establish a constant velocity (CV) kinematic model to describe its motion and the

system model is formulated as:

$$\mathbf{x}(k) = \mathbf{A}\mathbf{x}(k-1) + \mathbf{B}\mathbf{u}(k-1) + \mathbf{v}(k) \quad (3.51)$$

$$\mathbf{y}(k) = \mathbf{C}\mathbf{x}(k) + \mathbf{w}(k) \quad (3.52)$$

The system model can be understood as follows: Imagine the vehicle has been moving at constant velocity during the system period with the difference following the Gaussian distribution.

The system model consisting of the state transition matrix, the input gain (if any), the measurement matrix and noise covariances are all assumed to be known. Where  $T$  is the sampling interval and  $\mathbf{x}$  is the state of the vehicle which is given by

$$\mathbf{x} = \begin{bmatrix} x & \dot{x} & y & \dot{y} \end{bmatrix}^T \quad (3.53)$$

$$\mathbf{A} = \begin{bmatrix} 1 & T & 0 & 0 \\ 0 & 1 & 0 & 0 \\ 0 & 0 & 1 & T \\ 0 & 0 & 0 & 1 \end{bmatrix} \quad (3.54)$$

Assuming only position measurement is available, this yields the following measurement equation.

$$\mathbf{C} = \begin{bmatrix} 1 & 0 & 0 & 0 \\ 0 & 0 & 1 & 0 \end{bmatrix} \quad (3.55)$$

### 3.3.2.2 Constant Acceleration(CA)

If we have a priori knowledge that the vehicle moves at constant acceleration, we may establish a constant acceleration (CA) kinematic model to describe its motion and

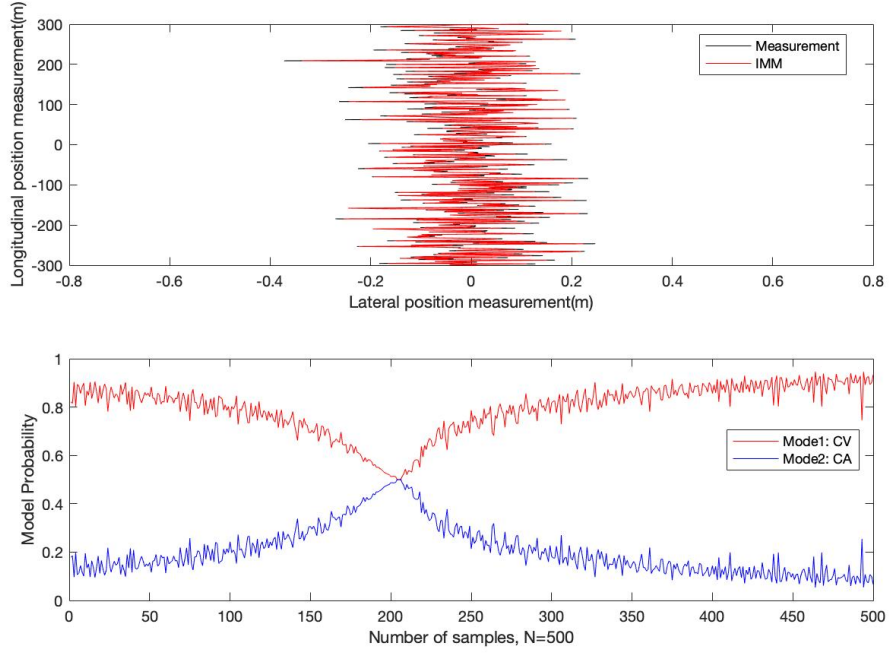


Figure 3.13: **Data is simulated using constant velocity model for a vehicle moving in straight line.** Model probability of two interactive multiple model filters are compared i.e. constant velocity and constant acceleration.

the system model is formulated as:

$$\mathbf{x}(k) = \mathbf{A}\mathbf{x}(k-1) + \mathbf{B}\mathbf{u}(k-1) + \mathbf{v}(k) \quad (3.56)$$

$$\mathbf{y}(k) = \mathbf{C}\mathbf{x}(k) + \mathbf{w}(k) \quad (3.57)$$

The system model can be understood as follows: Imagine the vehicle has been moving at constant acceleration during the current system period and follow the Gaussian distribution.

Where  $T$  is the sampling interval and  $\mathbf{x}$  is the state of the vehicle which is given by

$$\mathbf{x} = \begin{bmatrix} x & \dot{x} & \ddot{x} & y & \dot{y} & \ddot{y} \end{bmatrix}^T \quad (3.58)$$

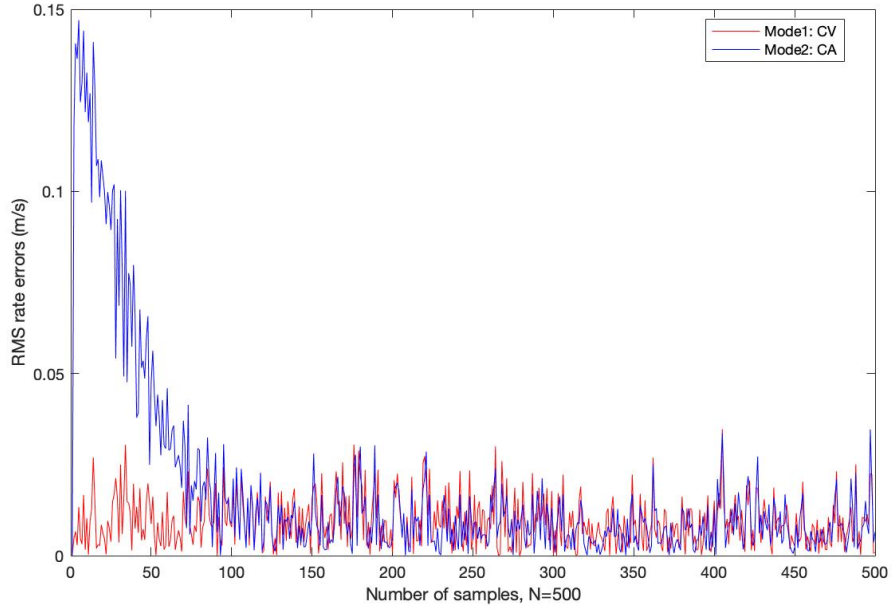


Figure 3.14: **Data is simulated using constant velocity model for a vehicle moving in straight line.** RMS rate error of constant velocity and constant acceleration are compared to number of samples ( $N=500$ ).

$$\mathbf{A} = \begin{bmatrix} 1 & T & \frac{T^2}{2} & 0 & 0 & 0 \\ 0 & 1 & T & 0 & 0 & 0 \\ 0 & 0 & 1 & 0 & 0 & 0 \\ 0 & 0 & 0 & 1 & T & \frac{T^2}{2} \\ 0 & 0 & 0 & 0 & 1 & T \\ 0 & 0 & 0 & 0 & 0 & 1 \end{bmatrix} \quad (3.59)$$

Assuming only position measurement is available, this yields the following measurement equation.

$$\mathbf{C} = \begin{bmatrix} 1 & 0 & 0 & 0 & 0 & 0 \\ 0 & 0 & 0 & 1 & 0 & 0 \end{bmatrix} \quad (3.60)$$

### 3.3.2.3 Coordinated Turn Model(CT)

The turn of vehicle moves usually follows a pattern known as coordinated turn which is characterized by constant turn rate and constant speed.

This model assumes that the turn rate is known or could be estimated. When the range rate measurements are available, the turn rate could be estimated by using range rate measurements. The tracking performance will be deteriorated when the assumed turn rate is far away from the true one. This model is usually used as one of the models in a multiple model's framework.

$$\mathbf{x}(k) = \mathbf{A}\mathbf{x}(k-1) + \mathbf{B}\mathbf{u}(k-1) + \mathbf{v}(k) \quad (3.61)$$

$$\mathbf{y}(k) = \mathbf{C}\mathbf{x}(k) + \mathbf{w}(k) \quad (3.62)$$

Where  $T$  is the sampling interval, turn rate  $\Omega(k)$  and  $\mathbf{x}$  is the state of the vehicle which is given by

$$\mathbf{x} = \begin{bmatrix} x & \dot{x} & y & \dot{y} & \Omega \end{bmatrix}^T \quad (3.63)$$

$$\mathbf{A} = \begin{bmatrix} 1 & \frac{\sin\Omega(k)T}{\Omega(k)} & 0 & \frac{1-\cos\Omega(k)T}{\Omega(k)} & 0 \\ 0 & \cos\Omega(k)T & 0 & -\sin\Omega(k)T & 0 \\ 0 & \frac{1-\cos\Omega(k)T}{\Omega(k)} & 1 & \frac{\sin\Omega(k)T}{\Omega(k)} & 0 \\ 0 & \sin\Omega(k)T & 0 & \cos\Omega(k)T & 0 \\ 0 & 0 & 0 & 0 & 1 \end{bmatrix} \quad (3.64)$$

Assuming only position measurement is available, this yields the following measurement equation.

$$\mathbf{C} = \begin{bmatrix} 1 & 0 & 0 & 0 & 0 \\ 0 & 0 & 1 & 0 & 0 \end{bmatrix} \quad (3.65)$$

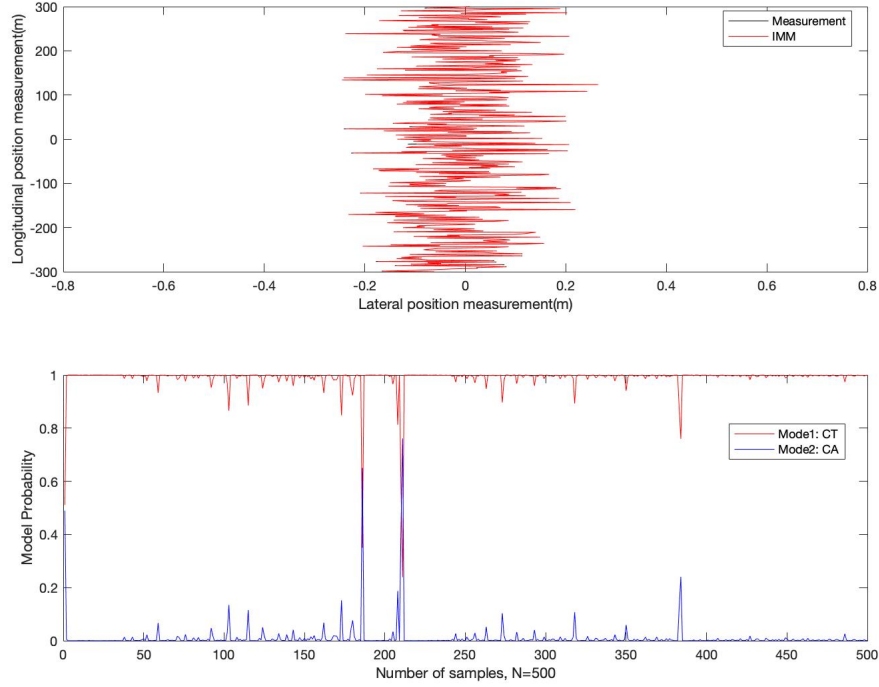


Figure 3.15: **Data is simulated using coordinated turn model for a vehicle moving in straight line.** Model probability of two interactive multiple model filters are compared i.e. coordinated turn and constant acceleration.

### 3.3.3 Performance Comparison

Design parameters for improving the performance of a multiple model filter for adaptive tracking can be accomplish by tuning state switching matrix and process noise selection.

#### 3.3.3.1 State switching matrix

This matrix  $p_{ij}$  defines the probability for the Markov chain that a object will make the transition from one filter model state to another state.

$$p_{ij} = \begin{bmatrix} p^{11} & p^{12} \\ p^{21} & p^{22} \end{bmatrix} = \begin{bmatrix} 0.9 & 0.1 \\ 0.1 & 0.9 \end{bmatrix} \quad (3.66)$$

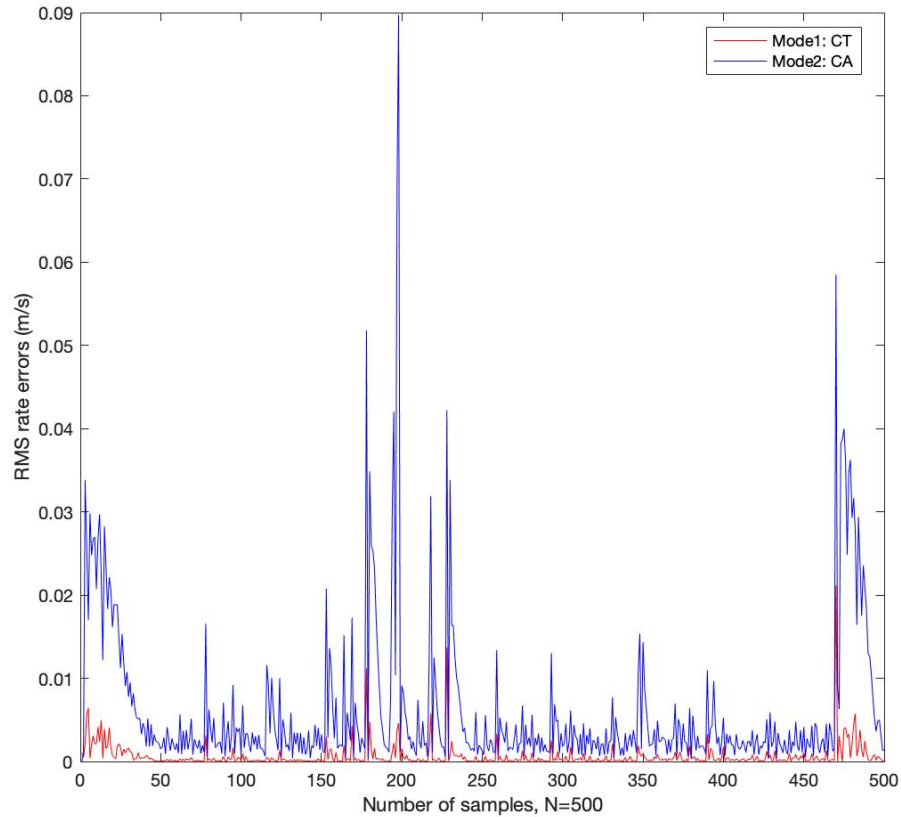


Figure 3.16: **Data is simulated using coordinated turn model for a vehicle moving in straight line.** RMS rate error of coordinated turn and constant acceleration are compared to number of samples ( $N=500$ ).

The state switching matrix is selected as part of the IMM algorithm to govern the underlying model switch probability. A comparison of varying values of matrix  $p_{ij}$  shows that the selection of the filter models has a larger effect on the state errors. The higher  $p_{11}$  will yield more peak error but lower root mean square error (RMSE) during the quiescent period. In general, the performance of the IMM appears to be relatively insensitive to the small changes in state switching matrix.

### 3.3.3.2 Process noise selection

Mixing filter model states and covariance in the IMM algorithm allows for a prompt reaction to dynamic models. However, this mixing will also affect the individual filter model gains. The right choice of noise levels will considerably improve the accuracy of detection. Similar to the state switching matrix, selection of the filter models has a larger impact on model performance than the selection of filter process noise.

### 3.3.4 Conclusions

Figure 3.13 and 3.14 was simulated using constant velocity model for a vehicle moving in straight line with a velocity of 50  $m/s$  along longitudinal axis. Figure 3.13 represents the trajectory travelled along with model probability of constant velocity and constant acceleration. It can be seen that since the trajectory was simulated using constant velocity model, the model probability of constant velocity is higher compared to its counterpart. This can be seen through graph where red represents constant velocity and blue is constant acceleration. Also figure 3.14 describes the RMS error plotted against number of samples ( $N=500$ ) this graph shows the error in constant acceleration exceeds the error in constant velocity and there is an abrupt increase in error during the beginning stage this gradually reduces as time progresses.

Similar explanation can be provided for, Figure 3.15 and 3.16 was simulated using coordinated turn model for a vehicle moving in straight line with turn rate  $\omega = 5$ . Figure 3.15 represents the trajectory travelled along with model probability of coordinated turn and constant acceleration. It can be seen that since the trajectory was simulated using coordinated turn model, the model probability of coordinated turn is higher compared to its counterpart. This can be seen through graph where red represents coordinated turn and blue is constant acceleration. Also figure 3.16 describes the RMS error plotted against number of samples ( $N=500$ ) this graph shows the error in constant acceleration exceeds the error in coordinated turn and there is

an abrupt increase in error during the beginning stage this gradually reduces as time progress with peak spikes in during few intervals.

The IMM approach computes the state estimate that accounts for each possible current model using a suitable mixing of the previous model-conditioned estimates depending on the current model. To obtain the best possible results, the IMM has to reduce the estimation errors during the uniform motion and maintain peak estimation error during the maneuver lower than that of detection of the maneuver. These results for the two model IMM illustrate that flexibility in modeling a dynamic motion. The overall IMM performance will at all times be similar to the best individual filter model within the IMM.

## 3.4 Bibliography

- [1] A. F. Genovese, “The interacting multiple model algorithm for accurate state estimation of maneuvering targets,” *Johns Hopkins APL technical digest*, 2001. pages 34, 42
- [2] Y. Bar-Shalom, X. R. Li, and T. Kirubarajan, *Estimation with applications to tracking and navigation: theory algorithms and software*. John Wiley & Sons, 2004. pages 42
- [3] Y. Bar-Shalom, K. C. Chang, and H. A. Blom, “Tracking a maneuvering target using input estimation versus the interacting multiple model algorithm,” *IEEE Transactions on Aerospace and Electronic Systems*, 1989. pages 42

# Chapter 4

## EXPERIMENTAL RESULTS AND DISCUSSION

### 4.1 Zero Velocity Detection

The detection of the swing and stance phase is decisive in providing feedback to Kalman filter, only when the person's foot is detected to be stationary on the ground. We implement a adaptive multi condition algorithm that complements the implementation by using gyroscope measurements.

The condition to declare a foot as stationary is given by:

$${}^s\mathbf{b}_g(k) = \begin{bmatrix} {}^s b_{gx}(k) \\ {}^s b_{gy}(k) \\ {}^s b_{gz}(k) \end{bmatrix} \quad (4.67)$$

$$|{}^s\mathbf{b}_g(k)| = \sqrt{{}^s b_{gx}(k)^2 + {}^s b_{gy}(k)^2 + {}^s b_{gz}(k)^2} \quad (4.68)$$

Where,  ${}^s b_{gx}(k)$ ,  ${}^s b_{gy}(k)$  and  ${}^s b_{gz}(k)$  being angular velocity measurements in the three axes given by the inertial unit during the data acquisition. In ideal conditions,

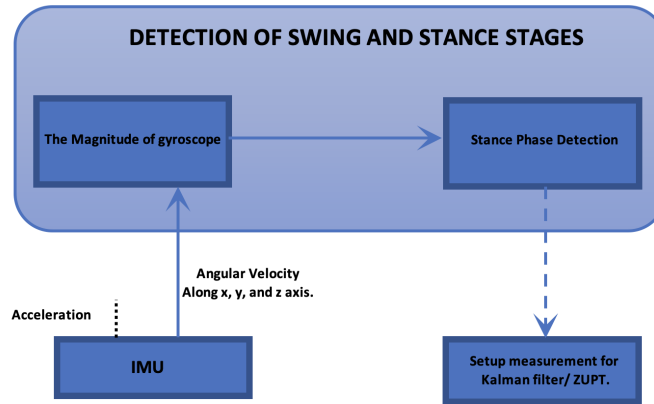


Figure 4.17: **Block diagram for swing and stance phase detection.** Angular velocity is examined for zero velocity detection.

this velocity should be zero in the stance phase. However, the total angular velocity will not be zero, but it should be lower than the given threshold. If this condition is true, it is considered that the foot is in stationary stance phase on the ground.

Figure 4.17 represents the block diagram for swing and stance phase detection using angular velocity. Where the magnitude of the gyroscope must be below a given threshold condition. Zero velocity detection occurs when the foot is stationary on the floor (totally still, or in a stance phase during walking). Once a stand still detection is obtained, the step-phase of the foot is known and consequently, the integration and correction of acceleration measurements can be done.

## 4.2 Zero Velocity Updates (ZUPTS)

Figure 4.18 depicts the block diagram of zero velocity update. Where both the accelerometer and gyroscope measurements are feed to inertial navigation. The INS transform the accelerations into the global frame, subtracts gravity from the vertical axis, and integrates twice (integrating acceleration gives us velocity; integrating velocity gives us position) to obtain velocity and position estimates. After applying the

zero-velocity detection and ZUPTs algorithm, the IMU based system is very accurate in measuring distance travelled. Zero Velocity Updates is one of the methods to reduce the drift in heading as gyroscope accumulates large errors in orientation due to the bias in the gyroscope measurements.

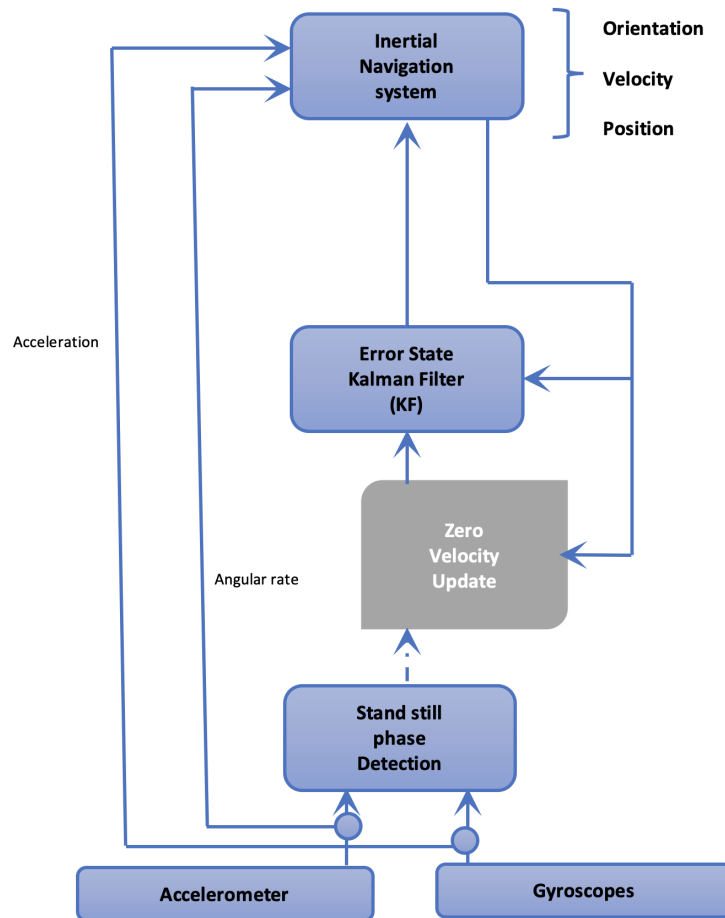


Figure 4.18: **Zero velocity update block diagram.** The block diagram illustrates the components and their relations of a ZUPT-aided INS system.

This method focusses on reducing drift without using any external infrastructure such as GPS nor map matching techniques. The Kalman filter is updated with velocity measurements by the ZUPTs strategy every time the foot is on the floor [1].

### 4.3 Description of the Data

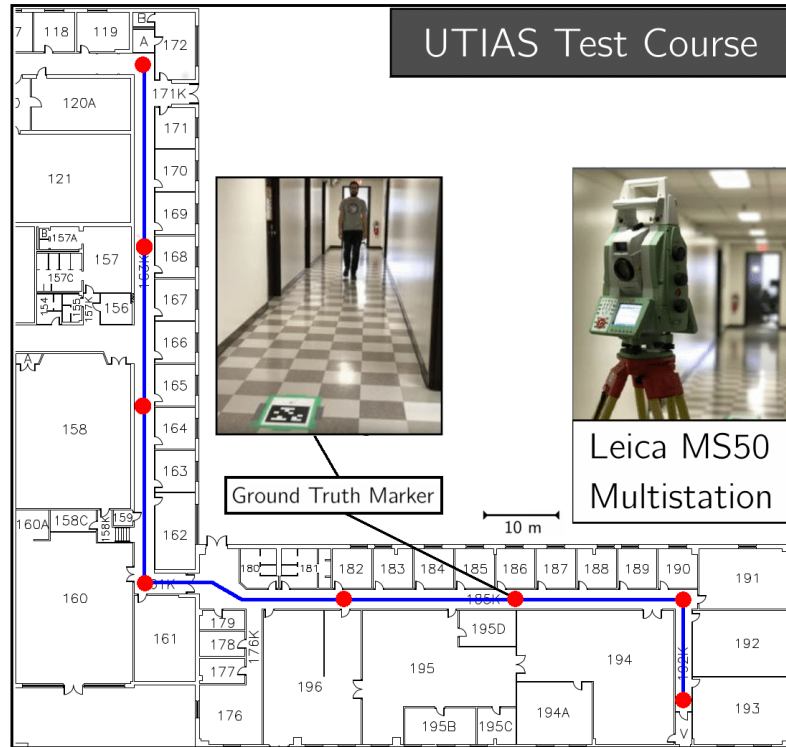


Figure 4.19: **Hallway Test Course.** Ground truth obtained using Leica M500 Multistation along with the marker [2].

Space and terrestrial autonomous robotic systems laboratory (STARS Lab) of university of Toronto has open-sourced foot-mounted inertial navigation dataset [2–4]. This consists of three different datasets as part of the complete dataset package for our experimental results we use the hallway dataset which incorporates walking and running motions through three connected hallways (with one-way distance of 110 m). The intermediate ground truth was obtained using a Leica M500 Multistation as shown in figure 4.19 and the VectorNav VN-100 inertial sensor unit was used to collect dataset at 200Hz. In total, 39 trials were collected, including data from five different test subjects.

In the coming section real-world data along with the ground truth are taken into

consideration to demonstrate the performance of the individual Kalman filter tracking for both walking and running model.

## 4.4 Demonstration of Pedestrian Tracking Using KF While Walking

We investigated the problem of tracking a pedestrian (Walking and Running framework) when zero velocity updates are applied on a foot-mounted pedestrian navigation system. With the help of commonly used detector i.e. the angular rate detector. Further, the results show that the performance varies between walking and running gait, where the proper work of the detector is questionable. We used gyroscope-based detection, as under given assumption, gyroscope-based detection clearly outperforms accelerometer-based detection, and that there is no significant improvement of the detector using both accelerometer and gyroscope data, over the one that employs signals from the gyroscope [5].

The following observations can be made to describe the performance of the proposed Kalman filter based ZUPT tracker in a walking framework.

- Figure 4.20 demonstrates the pedestrian tracking using KF based ZUPTs while walking it can be seen that the tracked trajectory precisely coincides with the ground truth trajectory as seen in figure 4.19. The difference in orientation occurs because we use Euler angle measurements for tracking orientation in three dimensions.
- It is found that for all the five different test subjects the tracking accuracy varied slightly using our proposed method this may be accounted for different individual motion pattern during walking (as there is slight variation in each and every human gait even when performing same motion in our case walking).
- Figure 4.20 represents walking framework with the threshold level equal to 0.6 it

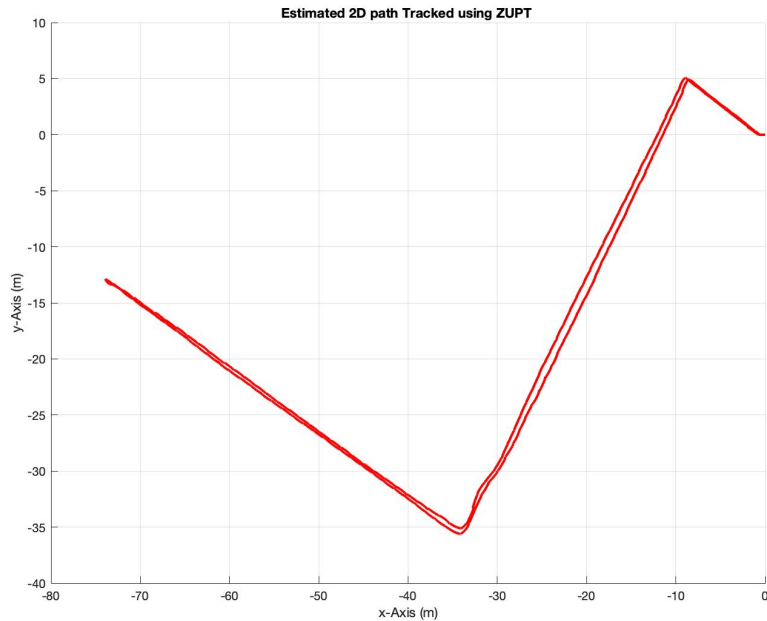


Figure 4.20: **Demonstration of Pedestrian Tracking Using KF While Walking.** Estimated two dimensional path tracked using ZUPT.

can be seen that the trajectory of walking almost matches with the trajectory provided as ground truth. The threshold may vary between individuals for same type of motion it is always best to determine the optimal threshold for a particular motion as well as for a particular individual to obtain best tracking results.

- Using figure 4.21 the total time taken for the experiment can be computed along with the total distance travelled. where, x-axis represents the total time take for the experiment and y-axis represents the distance travelled during the interval.
- It can also be noted that the total distance travelled during the entire experiment estimated to be 232.75 m whereas as per ground truth the total distance travelled should be equal to 220 m. The increase in distance might be accounted for false detection of zero velocity and ZUPTs.

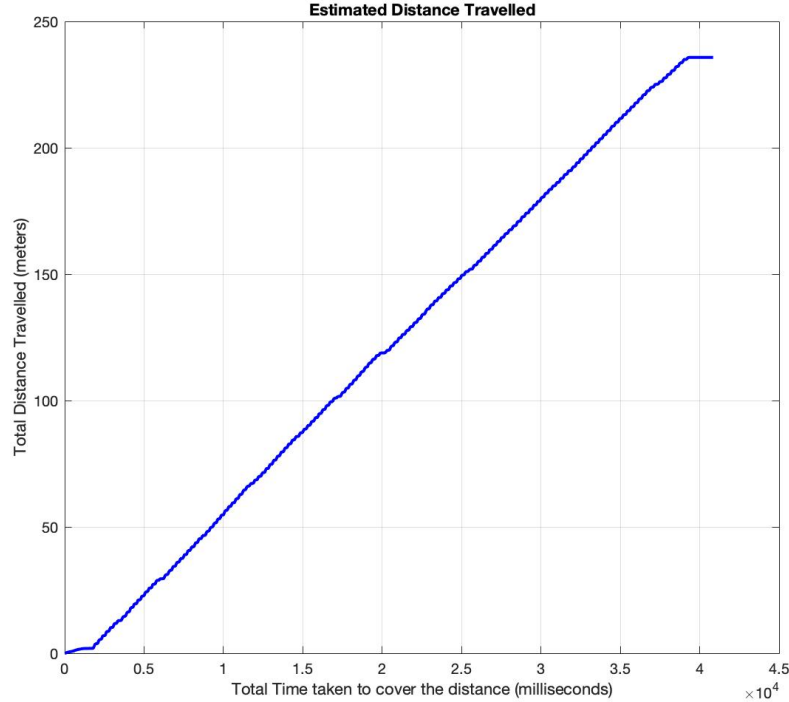


Figure 4.21: **Estimated Distance Travelled.** This graph represents total time taken  $v/s$  Total distance travelled for a walking framework.

## 4.5 Demonstration of Pedestrian Tracking Using KF While Running

The following observations were made to describe the performance of the proposed Kalman filter based ZUPT tracker while running. Similar conclusions can be drawn for running measurements.

- Figure 4.22 demonstrates the pedestrian tracking using KF based ZUPTs while walking it can see that the tracked trajectory precisely coincides with the ground truth trajectory as seen in figure 4.19. The difference in orientation occurs because we use Euler angle measurements for tracking orientation in three dimensions.

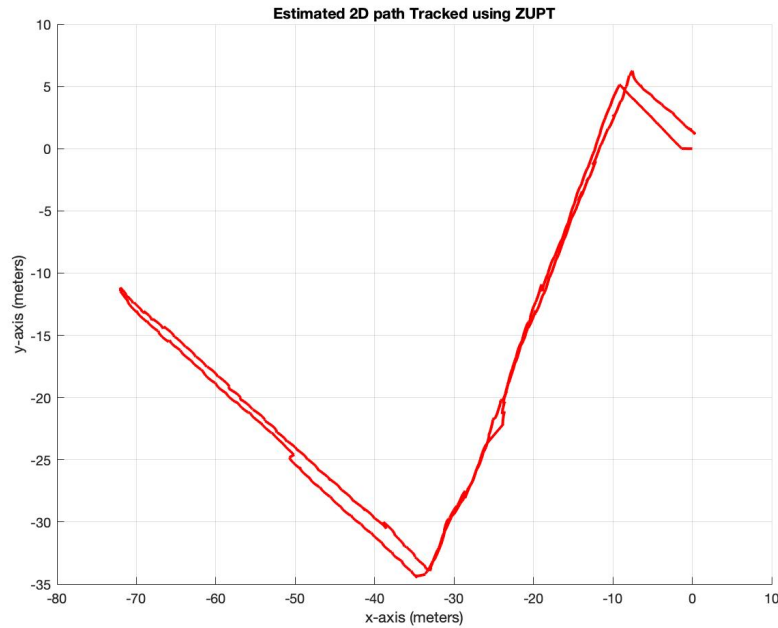


Figure 4.22: **Demonstration of Pedestrian Tracking Using KF While Running.** Estimated 2D path tracked using ZUPT.

- It is found that for all the five different test subjects the tracking accuracy varied slightly using our proposed method this may be accounted for different individual motion pattern during walking (as there is slight variation in each and every human gait even when performing same motion in our case walking).
- Figure 4.22 represents walking framework with the threshold level equal to 0.9 it can be seen that the trajectory of walking almost matches with the trajectory provided as ground truth. The threshold may vary between individuals for same type of motion it is always best to determine the optimal threshold for a particular motion as well as for a particular individual to obtain best tracking results.
- Using figure 4.23 the total time taken for the experiment can be computed along with the total distance travelled. where x-axis represents the total time take for the experiment and y-axis represents the distance travelled during the interval.

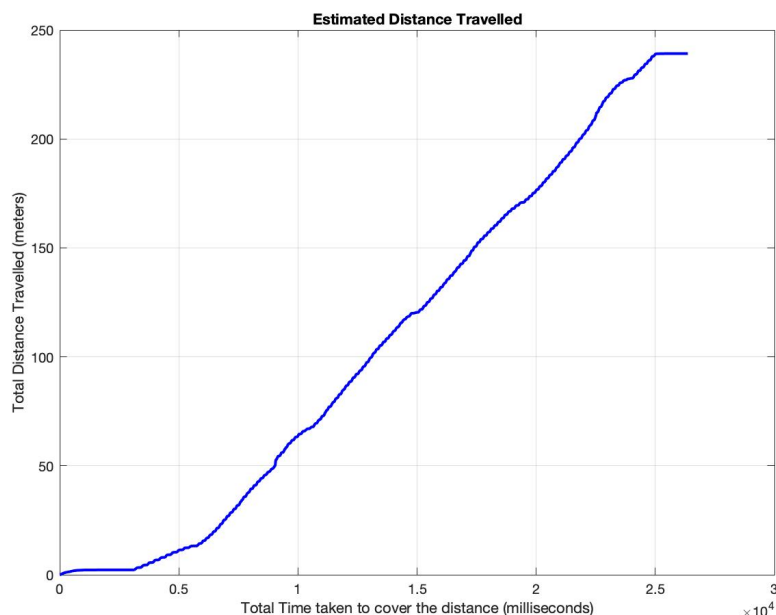


Figure 4.23: **Estimated Distance Travelled.** This graph represents total time taken v/s Total distance travelled for a running framework.

- It can also be noted that the total distance travelled during the entire experiment estimated to be 239.16 m whereas as per ground truth the total distance travelled should be equal to 220 m. The increase in distance might be accounted for false detection of zero velocity and ZUPTs.

## 4.6 Adaptive Tracking Using IMM Estimator

In this section we have suggested a methodology for improving the performance of foot-mounted ZUPT-aided inertial system using multiple model approach for dynamic motion. This study is restricted to the use of two models i.e. walking and running without using any external infrastructure such as GPS, building maps to correct the heading drift.

Finally, interactive multiple model can be applied to a dynamic system set-up giving achievable performance over a range of internal and external parameter.

The advantage of this approach is that a ZUPT-Kalman filter can be implemented to achieve competitive performance.

## 4.7 Bibliography

- [1] A. R. Jiménez, F. Seco, J. C. Prieto, and J. Guevara, “Indoor pedestrian navigation using an ins/ekf framework for yaw drift reduction and a foot-mounted imu,” in *2010 7th Workshop on Positioning, Navigation and Communication*, 2010. pages 2, 59, 70
- [2] B. Wagstaff and J. Kelly, “Lstm-based zero-velocity detection for robust inertial navigation,” in *2018 International Conference on Indoor Positioning and Indoor Navigation (IPIN)*, 2018. pages xii, 8, 60, 70
- [3] B. Wagstaff, V. Peretroukhin, and J. Kelly, “Robust data-driven zero-velocity detection for foot-mounted inertial navigation,” *IEEE Sensors Journal*, 2019. pages 60
- [4] B. Wagstaff, V. Peretroukhin, and J. Kelly, “Improving foot-mounted inertial navigation through real-time motion classification,” in *2017 International Conference on Indoor Positioning and Indoor Navigation (IPIN)*, 2017. pages 60, 70
- [5] I. Skog, P. Handel, J.-O. Nilsson, and J. Rantakokko, “Zero-velocity detection—an algorithm evaluation,” *IEEE transactions on biomedical engineering*, 2010. pages 8, 61, 70

# Chapter 5

## SUMMARY AND FUTURE WORK

This thesis investigated use of a multiple model estimator based adaptive indoor pedestrian tracking system for handling dynamic motion. In our proposed method, the dynamic motion consists of different human gait whose threshold is determined individually, and an interactive multiple model adjusts itself adaptively to correct the change in motion models. This chapter summarizes the main contribution of this research work along with recommendations for enhancing the indoor tracking capabilities.

### 5.1 Summary

The proposed method for indoor navigation of a pedestrian with dynamic motion can be modeled using interactive multiple model estimator. However, current modeling method uses two types of motion models they are running and walking. All other types of dynamic motion such as jogging, sprint, duck walking and climbing can be modeled by selecting a suitable thresholding technique using zero velocity detector and applying the ZUPT in a closed loop whenever the stand still position is detected.

Kalman filtering technique improving the accuracy of one type of motion accordingly the use of multiple model estimator like IMM covers and enhances the tracking capabilities for dynamic motion.

It can be noted that for one of the five test subject the pedestrian tracking using KF while walking the total distance travelled during entire experiment is estimated to be 232.75m whereas as per the ground truth it is equal to 220m also total estimated time taken for the experiment to be conducted is 41seconds. Similarly for pedestrian tracking using KF while running the total distance travelled during entire experiment is estimated to be 239.16m whereas as per the ground truth it is equal to 220m also total estimated time taken for the experiment to be conducted is 26.5seconds. It can also be noted that the error during running is large compared to walking as while running the target dynamics changes abruptly and the KF based system is not as accurate as while walking.

As mentioned earlier, the output of the system is influenced by the parameter selection such as error covariance matrix, state switching matrix and process noise selection. It is found that parameter selection needs to be considered for optimal performance. The results for dynamic filtering models show that using IMM algorithm provide the best overall results with respect to tracking. The filter model that is best matched to the pedestrian dynamics will provide the best state estimate and will have the highest probability. The overall IMM performance will at all times be similar to the best individual filter model within the IMM.

The results presented in this work confirmed that the multiple model estimator method can considerably improves the accuracy of the orientation, velocity and position estimate compared to single model detection using inertial sensor for a dynamic motion. A model of the pedestrian movement was designed, and the performance of the algorithm was evaluated on a real-world data. Further future work is required to assess the performance of the algorithm for a wider variety of motion models.

## 5.2 Future Work

The work presented in this thesis gives an insight into multiple model estimator for handling dynamic motion and fundamental approaches that will lead to the development of a more comprehensive indoor based pedestrian tracking system. This would eventually open up a number of leads for research. These leads will eventually help us in realizing the complete potential of inertial based systems. This section discusses some of the future work that will enable us to realize the complete potential of inertial based navigation systems.

- A method to detect normal and abnormal gait phase using a foot mounted IMU would help to precisely evaluating indoor navigation for an individual pedestrian. The focuses would be on identifying the gait sub-phases of normal and abnormal gaits using IMU attached to the foot of the pedestrian which would eventually help in determining the stand still phase of human gait [1].
- Detecting a stance phase of various motion models is proposed in order to perform velocity measurement update using machine learning as well as state estimation [2–5]. To achieve higher performance, the use of additional sensors is suggested. specifically, for climbing using a barometer which sense the change in pressure, is expected to increase the accuracy.
- Non-linear filter models can be used for localization such extended Kalman filter (EKF), unscented Kalman filter and particle filter to get higher accuracy as it is not feasible to estimate the tracking position for short duration [6, 7].
- This tracking algorithm can be used in other navigation systems with little or no modifications where the acceleration and angular velocity are of at most importance like in GPS aided navigation system for automobiles, air traffic control and space flights. The combination of GPS and inertial sensors improves the accuracy considerably [8, 9].

- Using quaternions as an alternate way to describe orientation or rotations in three-dimensional space compared to Euler angles they are simpler to compose and avoid the problem of gimbal lock. Therefore use of quaternions should improve the orientation estimation [10, 11].

Although, the work presented in this thesis has been developed for indoor navigation, it will be similarly applicable for developing a wearable technology in healthcare to monitor elderly and physically challenged, recreational activities, athlete training centre to make precise changes in improve their performance and handwriting reconstruction (As presented in appendix). Thus, the work presented in this thesis takes us a step closer in realizing multiple model tracking in general.

## 5.3 Bibliography

- [1] Y. C. Han, K. I. Wong, and I. Murray, “Gait phase detection for normal and abnormal gaits using imu,” *IEEE Sensors Journal*, 2019. pages 70
- [2] I. Skog, P. Handel, J.-O. Nilsson, and J. Rantakokko, “Zero-velocity detection—an algorithm evaluation,” *IEEE transactions on biomedical engineering*, 2010. pages 8, 61, 70
- [3] S. Y. Park, H. Ju, and C. G. Park, “Stance phase detection of multiple actions for military drill using foot-mounted imu,” *sensors*, 2016. pages 8, 70
- [4] J. Callmer, D. Törnqvist, and F. Gustafsson, “Probabilistic stand still detection using foot mounted imu,” in *2010 13th International Conference on Information Fusion*, 2010. pages 70
- [5] B. Wagstaff and J. Kelly, “Lstm-based zero-velocity detection for robust inertial navigation,” in *2018 International Conference on Indoor Positioning and Indoor Navigation (IPIN)*, 2018. pages xii, 8, 60, 70
- [6] B. Wagstaff, V. Peretroukhin, and J. Kelly, “Improving foot-mounted inertial navigation through real-time motion classification,” in *2017 International Conference on Indoor Positioning and Indoor Navigation (IPIN)*, 2017. pages 60, 70
- [7] A. R. Jiménez, F. Seco, J. C. Prieto, and J. Guevara, “Indoor pedestrian navigation using an ins/ekf framework for yaw drift reduction and a foot-mounted imu,” in *2010 7th Workshop on Positioning, Navigation and Communication*, 2010. pages 2, 59, 70
- [8] H. Qi and J. B. Moore, “Direct kalman filtering approach for gps/ins integration,” *IEEE Transactions on Aerospace and Electronic Systems*, 2002. pages 29, 70

- [9] J. Farrell, *Aided navigation: GPS with high rate sensors*. 2008. pages 70
- [10] K. Shoemake, “Animating rotation with quaternion curves,” in *Proceedings of the 12th annual conference on Computer graphics and interactive techniques*. pages 71
- [11] J. C. Chou, “Quaternion kinematic and dynamic differential equations,” *IEEE Transactions on robotics and automation*, 1992. pages 71

# Appendices

# Appendix A: Handwriting Reconstruction using Inertial Sensors

This appendix presents a handwriting trajectory reconstruction method based on which a user can input gestures in three-dimensional space. In order to track the trajectory of handwriting using smartphone with inertial sensors, the three-axis accelerometer and three-axis gyroscope measurements from an inertial measurement unit are recorded. These measurements from inertial sensor are filtered, removing the bias along with attenuating drift and noise using complementary filter which reduces low and high frequency noises of the signals. Figure 24 depicts the advantage of using low pass filter for accelerometer data as it reduces the jitter noise also figure 25 shows that the use of high pass filter for gyroscope measurements reduces the drift along all the three coordinate axis.

For this experiment smartphone (Google Pixel 3) with MEMS inertial sensor was used. A trajectory estimation algorithm is employed to convert measurements into a trajectory on 2-D plane. The data from the inertial sensor were filtered and a zero-velocity update is implemented in a close loop system, for a Kalman filter that estimates the errors in the orientation, velocity and position. The orientation is expressed in Euler angles which is the main reason why the orientation is not aligned.

The employment of inertial sensors enables users to draw gestures in almost any

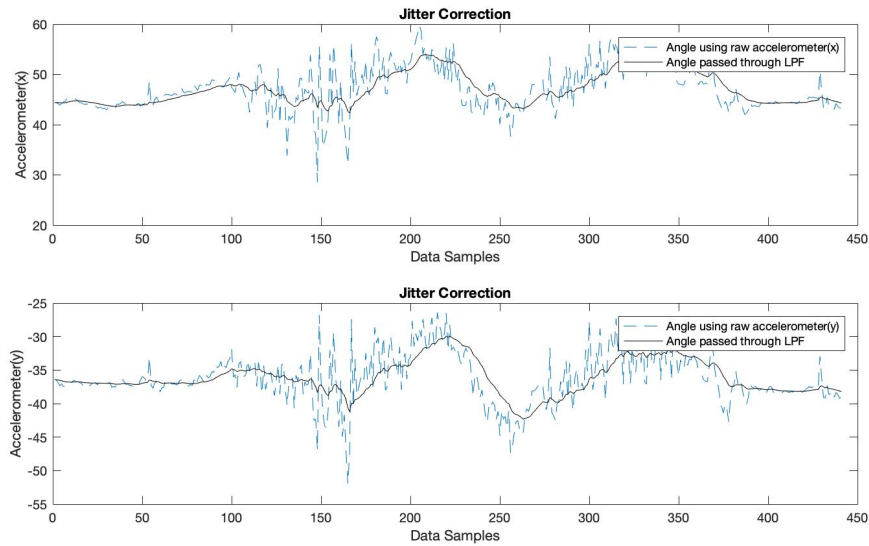


Figure 24: **Accelerometer data passed through low pass filter.** Accelerometer measurements when passed through low pass filter helps in improving jitter correction.

place because they do not require any external reference devices. The shapes look somewhat distorted from representative gesture shapes as there is increment in time the integration error also increases. Also, shapes of different classes look distinguishable among one another. The future work is to enhance the preprocessing step of the estimated trajectories and to design gesture shapes more convenient to users. The experimental results of our algorithm are presented in figure 26 .

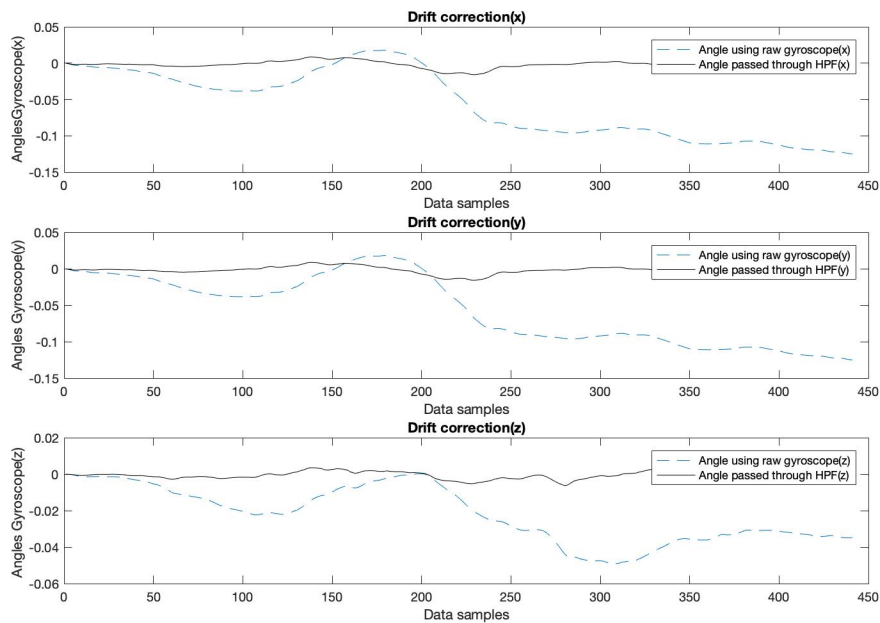


Figure 25: **Gyroscope data passed through high pass filter.** Gyroscope measurements when passed through high pass filter helps in correcting the drift.

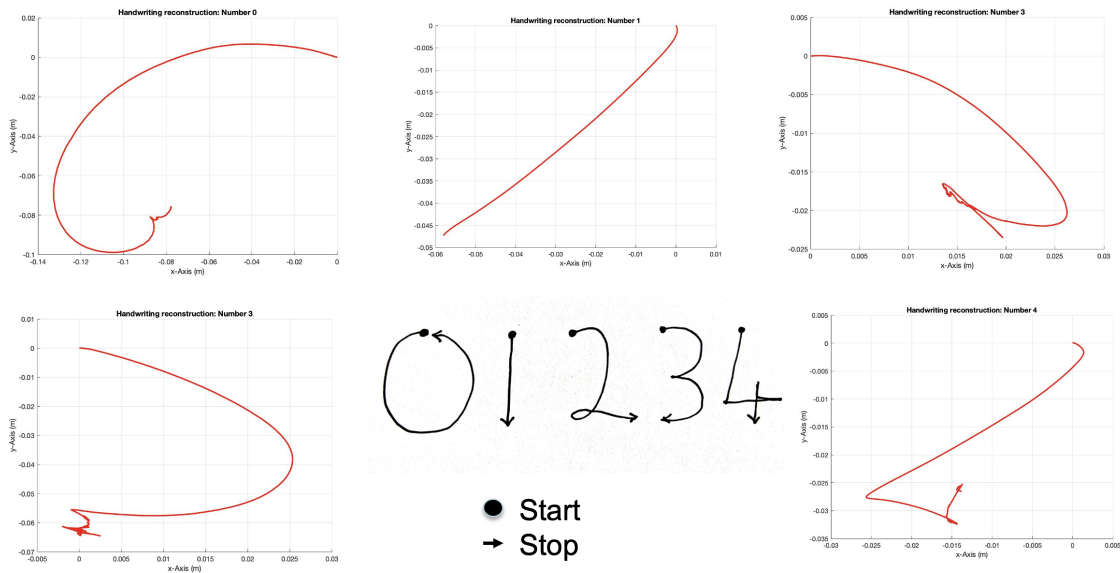


Figure 26: **Gesture Reconstruction.** Experimental results of our proposed method for handwritten number reconstruction.

# Vita Auctoris

NAME: Ravindra Kumar Dhanapal

PLACE OF BIRTH: Tamil Nadu, India

YEAR OF BIRTH: 1994

EDUCATION: Kendriya Vidyalaya Hebbal,  
Bengaluru, India  
2012, Secondary Education  
PCMB- Physics, Chemistry, Mathematics and Biology

Visvesvaraya Technological University,  
Bengaluru, India  
2016, Bachelor of Engineering  
Electrical and Electronic Engineering

University of Windsor, Windsor, Ontario  
2020, Master of Applied Science  
Electrical and Computer Engineering